Explosive properties of water in volcanic and hydrothermal systems

R. Thiéry

Laboratoire Magmas et Volcans, UMR 6524, CNRS/Clermont Université, Clermont-Ferrand, France

L. Mercury

Institut des Sciences de la Terre d'Orléans, UMR 6113, CNRS/Université d'Orléans, Orléans, France

R. Thiéry, Laboratoire Magmas et Volcans, UMR 6524, CNRS/Clermont Université, 5 rue Kessler, F-63038 Clermont-Ferrand Cedex, France

L. Mercury, Institut des Sciences de la Terre d'Orléans, UMR 6113, CNRS/Université d'Orléans, 1A, rue de la Férollerie, F-45071 Orléans Cedex, France

Abstract. This paper describes, from a thermodynamic point of view, the physico-chemical conditions, under which water behaves as an explosive. This phenomenon occurs frequently in hydrothermal and volcanic systems, when water is brutally shifted from its initial equilibrium state. Water (either liquid or gas) becomes metastable or unstable, and reequilibrates by violent demixing of a liquid-gas mixture. In a first step, a phenomenological approach of metastability is given in an one-component perspective, introducing the notion of spinodals and delimiting the extent of metastable fields. The physical mechanisms (bubble nucleation, cavitation, spinodal decomposition), which are involved in these explosive transformations of water, are detailed in what relates to the natural eruptions topic. The specific thermodynamic properties (P-v-T-H-U) of metastable water are presented by using the reference Wagner and Pruss equation of state. Then, the mechanical work produced by the different possible physical transformations, including decompression, vaporization, isobaric heating and exsolution, involved in water explosions are quantified. The classic calculation of the energy balance under the reversible assumption is here extended proposing a pathway to take irreversibility into account. This model can be used to estimate magnitude of volcanic impacts from scaling laws based on explosion energies.

1. Introduction

Magmatic, volcanic and hydrothermal systems are characterized by an explosive release of energy, which is produced essentially by the mechanical work of expansion of fluids. This explosivity is firstly caused by the exsolution of juvenile, hot and pressurized fluids, mainly composed of water (> 80% by volume) [*Mills*, 2000], during the magma crystallization and ascent through the crust. This feature is best visualized by the drastic increase of the volumetric fraction (f_v) of exsolved water at near-surface conditions of the Earth (Figure 1), where f_v is computed from the mass fraction of exsolved water (wt % H_2O) by:

$$\text{wt \% } H_2O = \frac{\rho_w \, f_v}{\rho_w \, f_v + \rho_m \, (1 - f_v)}, \tag{1}$$

with ρ_m being the magma density ($\rho_m \simeq 2500$ kg/m^3) and ρ_w, the density of the aqueous phase (in kg/m^3) calculated by the *Wagner and Pruss* [2002] equation of state for water. As pointed out by *Burnham* [1979], more than 3 Gm^3 of steam can be produced from only one Gm^3 of magma exsolving 2 wt % of water at 100 bar. Such a fluid volume cannot be retained on a long period of time under surface, and one of the essential questions of volcanic processes is the evacuation of this excess water out of magmas. The main factor controlling the gas removal is the viscosity of magmas, giving a wide range of contrasted behaviours, from strombolian fountaining to the violent plinian explosions. The most explosive (and sometimes cataclysmic) volcanism arises at the conjunction of both factors, i.e. high water content and high magma viscosity. Figure 1 shows also that the increase of the water volume fraction is accompanied by a marked change of the magma nature, where the silicate melt is fragmented into an aerosol of ash and steam.

Obviously, this transition occurs when the water volume fraction overruns some threshold, which was approximated ca. 50 % by *Wohletz et al.* [1984] or 75-84 % by *Sparks* [1978]. However, recent experimental and theoretical studies [*Thomas et al.*, 1994; *Zhang et al.*, 1997; *Zhang*, 1999; *Spieler et al.*, 2004] have demonstrated the influence of others factors, like the depressurization rates and intensities, the melt viscosities, surface tensions or gas diffusivities on the fragmentation onset. Anyway, this catastrophic exsolution occurs either in the sommital parts of the magmatic chamber just before the eruption, or in the vent during the eruption. The rapid exsolution, decompression and blowing out of these magmatic chambers filled with fluid-rich magmas, leads to the ejection of huge amounts of gas and tephra (pumice and ash), development of pyroclastic falls, flows or surges, and finally, the collapse of a caldera.

The second main cause of explosive eruptions is due to the presence of cold liquid water on the Earth surface. Sudden mixings of large quantities of non-juvenile liquid water with hot materials produce violent explosions, giving rise to a large number of various explosive phenomena (hydroeruptions, [*Moyer and Swanson*, 1987]; surtseyan volcanism, [*Kokelaar*, 1986]; phreato-magmatic eruptions including hydrothermal geysering, [*Browne and Lawless*, 2001]). Additionally, hydrothermal eruptions are not the simple result of liquid water heating, but also require the incidental and sudden decompression of pressurized waters, which are close to their boiling conditions.

Thus, water is the main explosive agent on Earth. For this reason, the properties of water have been the subject of numerous studies, both experimental and theoretical [*Wohletz*, 1983, 1986, 2002; *Zimanowski et al.*, 1991, 1995, 1997b]. In particular, the explosions of water in contact with magma are usually explained by complicated physico-chemical

mechanisms, usually termed "Molten-Fuel-Coolant Interactions" (MFCI) [*Wohletz*, 1983; *Theofanous*, 1995; *Zimanowski et al.*, 1997a]. Despite the abundant litterature, mainly in the volcanological, physico-chemical or industrial engineering fields, these processes are so complex that they are not well understood yet.

In a first part, we will show how water explosions can be described in a general theoretical framework of fluid metastability [*Debenedetti*, 1996]. The notions of so-called spinodal curves, superheated liquids, supercooled gas and others will be introduced, and we will see how these concepts, originating from fundamental physics of fluids, can be useful to understand these eruptive phenomena. Next, the physical mechanisms involved in explosive water reactions will be detailed in what may be used by the volcanological community. Then, the five main energetical contributions involved in magma–water interactions, which are respectively (1) decompression, (2) vaporization, (3) liquid heating, (4) steam heating and (5) magma exsolution, will be quantified by using the reference equation of state for water of *Wagner and Pruss* [2002]. The part of the magmatic thermal energy, which can be transformed into explosive kinetic energy, will be analysed. This will help us to differentiate the different types of hydrothermal and volcanic environments as a function of their explosion energy, calculated according to the one-component water case. Finally, we will show how our model can be used to estimate the intensity of volcanic explosions with the help of scaling laws.

2. What Makes Water an Explosive ?

An explosion is always the violent response of a system to a physico-chemical perturbation, which has left it in an energetic, metastable or unstable, state. For instance, fast thermodynamic processes (water heated at the contact of a magma, rapid depressurisation

of a liquid, high-speed flow of a fluid, ...) produce highly transient metastable states, which return towards equilibrium in a very rapid and explosive way. In other words, metastable states are temporary configurations, which are more or less distant from an equilibrium state. The more important is this distance (i.e. the metastability degree), the more explosive will be the relaxation towards equilibrium. As a consequence, the characterization of metastable states can gives us some indications about the explosive feature of physico-chemical transformations.

This paper follows a phenomenological approach, based on classical thermodynamics and equations of state. This introduces the notion of spinodals, which are the theoretical bounds between metastability and instability.

2.1. A Phenomenological Approach of Metastability

The thermodynamic properties of a pure substance is described by an equation of state, which is usually formulated by means of a mathematical formulation of the Helmholtz free energy A, as a function of the temperature T and molar volume v for pure fluids:

$$A = A(T, v). \tag{2}$$

Any thermodynamic parameter can then be obtained by simple differentiation of the $A(T, v)$ function of adequate order [*Thiéry*, 1996].

Variables T and v are independent, but one important consequence of the second law of thermodynamics is that some sets of (T, v) values are not allowed. Indeed, to be at internal equilibrium, a fluid of given (T, v) must obey the following relations [*Debenedetti*, 1996]:

$$\left(\frac{\partial T}{\partial S}\right)_P > 0, \tag{3}$$

where S is the entropy; and,

$$\left(-\frac{\partial P}{\partial v}\right)_T > 0. \tag{4}$$

Equation 3 is commonly referred to as the thermal stability criterion, and equation 4 as the mechanical stability criterion. Thus, the (T, v) space of a pure compound is splitted into three main regions (Figure 2):

1. the instability field, where neither the thermal nor the mechanical stability criteria 3 and 4 are satisfied. The incidental formation of a fluid with (T, v) properties in the unstable field will be immediately followed by its explosive demixion into a biphasic liquid-gas mixture by a process of spinodal decomposition ([*Debenedetti*, 2000], see Section 2.2).

2. the metastability field, where the fluid phase obeys the stability criteria, but appears to be less stable than a biphasic association. Demixing of the initial fluid (either by partial vaporization or condensation) will proceed by means of nucleation processes (see Section 2.2). The metastable and unstable regions are separated by the spinodal curves. The first spinodal, noted Sp(L), is the liquid spinodal, and is the limit of a metastable (superheated) liquid; whereas the second spinodal, noted Sp(G), is the gas spinodal, limiting the metastable (supercooled) gas field. Both spinodals meet at the critical point.

3. and the stability field, where the fluid is fully stable. Metastable and stable fields are delimited by the binodal curve.

Metastable fields can also be depicted in a (P, T) diagram (Figure 3). The liquid spinodal starts from the critical point and runs to lower pressures with decreasing tempera-

tures (at least, up to 330 K where the liquid spinodal curve exhibits a pressure minimum, see [*Imre et al.*, 1998] for further details about the topology of the liquid spinodal curve of water). It is worth to note that the liquid spinodal curve runs through the region of negative pressures. As a matter of fact, any condensed material can indeed support negative pressures. Thus, the liquid spinodal curve indicates the highest (theoretical) tensile stresses that a liquid can bear out. This property of water (and other liquids) has been well demonstrated by experimental studies of aqueous fluid inclusions [*Zheng*, 1991; *Zheng et al.*, 1991; *Shmulovich et al.*, 2009]. Note that the field of negative pressure relates only to the liquid, as negative pressure for gases is a nonsense (due to pressure-density proportionality, zero gas pressure corresponds to vacuum).

The representation of thermodymanic properties of a fluid in the metastable region is a highly demanding task for an equation of state, firstly because of the divergence of some thermodynamic variables (for instance, the isobaric heat capacity), and secondly because of the scarcity of experimental data. The equation of state of *Wagner and Pruss* [2002] has been selected, as it is well acknowledged by the scientific community for the liability of its extrapolation in the metastable field (see [*Wagner and Pruss*, 2002], where its validity for superheated liquid water is fully discussed). Note however that the equation of state of *Wagner and Pruss* [2002] yields meaningless results in the unstable field, and care must be taken to avoid this domain, in particular, for the calculations of spinodals.

2.2. Nucleation-Growth and Spinodal Decomposition

The distinction between metastable and unstable states is closely linked to the type of relaxation mechanism towards equilibrium. Metastable systems re-equilibrate themselves by nucleation and phase growth, whereas unstable ones proceed to equilibrium by spin-

odal decomposition [*Debenedetti*, 1996, 2000]. This distinction between nucleation and spinodal decomposition is important, as this will control many parameters, such as the incubation time before relaxation, the final distribution of matter, the kinetic rate of the transformation, the rate of energy release and hence its explosivity.

Nucleation and spinodal decomposition are both the results of fluctuations of an order parameter (i.e. the fluid density for a pure system) describing the system at the microscopic scale. Modalities of phase separation are totally different between these two mechanisms.

Spinodal decomposition does not require any thermal activation energy: it is a spontaneous process, which occurs as soon as the system enters the unstable domain. Inversely, nucleation is an activated process, which will take more or less time to occur in a metastable system.

Nucleation is produced by a localized high-amplitude fluctuation of the density. The growth of a small nucleus entails an energy cost as long as a critical size is not attained. The energy barrier E_b, which has to be overcomed for a critical radius r_c, can be approximated by the classical nucleation theory (e.g. [*Debenedetti*, 1996]):

$$E_b = \frac{16\,\pi\,\sigma^3}{3\,(P_{\rm vap} - P_{\rm liq})^2}, \tag{5}$$

$$r_c = \frac{2\,\sigma}{|P_{\rm vap} - P_{\rm liq}|}, \tag{6}$$

where σ is the surface tension between liquid and gas, $P_{\rm vap}$ and $P_{\rm liq}$ are respectively the pressure in the gas and liquid phases. The important control parameter is $|P_{\rm vap} - P_{\rm liq}|$, which increases from zero at saturation conditions to large values at spinodal conditions. Thus, nucleation is facilitated, when both E_b and r_c become sufficiently small, giving rise

to the process of homogeneous nucleation. Thermodynamic spinodal corresponds to nil E_b. Homogeneous nucleation becomes spontaneous as soon as E_b is of the same magnitude order than thermal fluctuations: this is the kinetic spinodal limit [*Kiselev*, 1999; *Kiselev and Ely*, 2001], whose curve follows roughly, but shifted at lower temperatures and higher pressures, the theoretical liquid spinodal curve Sp(L) in a (P,T) diagram [*Shmulovich et al.*, 2009]. At any condition between saturation and the kinetic spinodal curve, nucleation occurs only at some favourable sites, produced by impurities in the fluid or along solid surfaces, where the energy barrier is considerably lowered. This nucleation process is well known under the name of heterogeneous nucleation (e.g. [*Lasaga*, 1998]).

Conversely, spinodal decomposition is produced by low-amplitude density fluctuations between adjacent regions in the fluid: slightly more dense domains evolve towards a liquid-like density, and less dense regions evolve towards a gas-like density [*Debenedetti*, 1996, 2000]. Because this process involves also the creation of liquid-gas interfaces (which is expensive in energy), only regions of long wavelengths (i.e. covering large areas for a minimal surface cost) will be favoured by these density evolutions at the expense of smaller domains, which will shrink away.

In other words, spinodal decomposition is the separation of regions, whose densities are progressively evolving towards two poles, liquid and gas, until stable conditions are reached, whereas nucleation-growth is the formation of new regions from the nucleation sites, but presenting a net density contrast with their surroundings since the beginning.

In the case of spinodal decomposition, phase separation occurs throughout the material, whereas phase splitting for nucleation arises only at some nucleation sites and proceeds by means of a reactive interface (either a boiling front or a condensation surface). This

implies slower transformation rates for nucleation-growth, as the growth of the newly nucleated phases requires longer pathways for heat and/or mass transfer. Therefore, the heat and/or mass diffusion may be critical limiting parameters in the nucleation-growth process. On the contrary, spinodal decomposition of liquids into vapours is particularly explosive, as it is accompanied by a partial vaporization and an important energy release in a very short lapse of time. Table 2 summarizes the main differences between these two fundamental kinetic processes of phase separation, which are nucleation-growth and spinodal decomposition. It is worth to note that both mechanisms are not mutually exclusive: a reequilibration transformation of a high-disequilibrium state can start with spinodal decomposition, and then proceed further by the classical mechanism of nucleation-growth. Because the spinodal decomposition of fluids into liquid-gas mixtures is a very rapid process, it cannot be studied experimentally [*Nonnenmacher*, 1980; *Debenedetti*, 2000], except at conditions, which are very close to the critical point.

Very rapid changes of thermodynamic conditions are needed to initiate explosive physical transformations by spontaneous nucleation or spinodal decomposition: these are treated in the next section.

2.3. The Explosive Physical Transformations of Water

Different physical transformations can lead to explosive phenomena (Figure 3): the explosion intensity can be, indeed, visualized by considering the relative positions between the spinodals and the $P-T$ paths undergone by the fluid.

2.3.1. Rapid Heating of Liquid Water

The fortuitous contact of liquid water with a hot surface (at the microscopic scale) is the first way to trigger an explosive boiling. It mainly relates to (1) explosive water-

magma interactions [*Wohletz*, 1986; *Zimanowski et al.*, 1986, 1991, 1995; *Wohletz*, 2002], and to (2) steam explosions caused by water spills onto molten metals or salts [*Reid*, 1983]. To a first step, all of these processes can be approximated by isobaric heating transformations, i.e. by a horizontal line in the $P-T$ phase diagram of Figure 3, running from the stable liquid field up to the metastable or unstable regions. Extensive laboratory investigations have demonstrated that the boiling temperature T_b of water is the main parameter controlling its explosivity [*Reid*, 1983]: indeed, most explosive boilings are obtained when T_b is, roughly, either around T_{hn} or T_L [*Reid*, 1983]. T_{hn} refers to the temperature of homogeneous nucleation, or the temperature of superheating limit. A value of 577 K (304°C) is usually accepted for the temperature T_{hn} of water at one bar [*Reid*, 1983]. T_L is the Leidenfrost temperature [*Leidenfrost*, 1756], at which a thin and stable vapour layer forms at the interface between the hot body and liquid water. Above T_L, this stable vapour layer film constitutes an insulating zone, which prevents any explosion [*Mills*, 1984]. However, a mechanical shock can force contact between liquid water and the hot body, and trigger a violent thermohydraulic explosion [*Zimanowski et al.*, 1991]. A precise and definite value for T_L cannot be given, as it depends on the physical properties of the hot surface, such as its thermal diffusivity, its surface roughness, its prefragmented state and others. Nevertheless, T_L is below the critical temperature T_c of water, and may be as high as the liquid spinodal temperature $T_{\rm sp}$ at 1 bar, ($T_{\rm sp} = 320.45°C = 593.6$ K). Hence, explosive water boilings occur either by spontaneous homogeneous nucleation or by spinodal decomposition. In this latter case, nucleated boiling does not succeed to keep the pace to evacuate the excess heat: this results to a thermal shock and to the spinodal decomposition of the interfacial liquid water.

2.3.2. Liquid Decompressions

Another important cause of fluid instabilities is the rapid depressurization of a liquid, whose $P-T$ path in Figure 3 is represented by a descending vertical line up to a final pressure P_f. But depending upon the initial liquid temperature T_i, this pressure drop can lead to two contrasted evolutions, which we will define as (1) superspinodal decompression and (2) subspinodal decompression. The first case is a decompression in the subcritical region, where the $P-T$ depressurization path cuts the kinetic liquid spinodal in a temperature range, let's say between 250°C ($\simeq 0.8\,T_{hn}$) and T_c, the critical temperature of water ($T_c = 374$°C). As a consequence, the liquid state goes through the metastable field, and subsequently through the unstable field. Such an evolution, which is very rapid, results finally to an explosive vaporization through spinodal decomposition or spontaneous nucleation, which we call a superspinodal decompression.

The second case is a pressure drop of a liquid up to 1 bar, but at a temperature below 250°C. At the difference of the former case, the $P-T$ decompression path does not crosscut the liquid spinodal curve and will produce either non-explosive or moderately explosive boiling, which we refer to as a subspinodal depressurization. This last situation may be also at the origin of cavitation (see next section).

Thus, spinodals are useful to assess the explosive character of a transformation, a conclusion already inferred by engineers dealing with the failure of containers of pressurized liquids. The most serious damages occur, as a rule of thumb, when the temperature of the liquid reservoir is between $0.9\,T_c$ (i.e. roughly $T_{\rm sp}$) and T_c. Such explosions are called BLEVEs, for Boiling Liquid Expanding Vapour Explosions [*Birk and Cunningham*, 1996; *Casal and Salla*, 2006; *Salla et al.*, 2006; *Abbasi and Abbasi*, 2007]. From this temperature

range, one can estimate that the violence of these explosions may be explained, at least in the very first steps, by the spinodal decomposition of superheated liquids induced by a sudden depressurization.

This distinction between subspinodal and superspinodal decompressions may have profound implications on the functioning of hydrothermal systems, as they are subjects to recurring pressure drops up to their lower external pressure P_{ext}. For continental hydrothermal systems, P_{ext} is the atmospheric pressure, whereas for oceanic systems, P_{ext} is the pressure of the sea bottom (mainly between 100 bar and 500 bar for sea floors between 1000 m and 5000 m). Superspinodal liquid depressurizations may occur in eruptions of continental high-temperature and liquid-dominated hydrothermal fields (whose temperatures typically exceed 250°C). The conditions of the largest known hydrothermal eruptions in New Zealand are not known precisely, but maximal explosion focal depths have been estimated up to 450 meters [*Browne and Lawless*, 2001]. This implies incipient boiling at 260°C and 45 bars, i.e. favourable conditions for a nearly superspinodal depressurization against the atmospheric pressure. Phreato-magmatic eruptions produced by deep maar-diatreme systems may also be linked to superspinodal decompressions. To the contrary, subspinodal decompressions are produced by low-temperature continental hydrothermal fields (initial temperature T_i below 250°C) and oceanic hydrothermal fields (final pressure P_f mostly above the spinodal pressure P_{sp}), producing less explosive phenomena, like geysering and biphasic liquid-gas discharges. The contrasted behaviour between subspinodal and superspinodal systems may explain the large temperature difference between oceanic and continental hydrothermal systems. Oceanic hydrothermal fields typically discharge fluids between 300 and 400°C, whereas the temperatures of fluids in continental geothermal

fields are lower, mainly between 100°C and 225°C [*Lee*, 2001]. Both mentioned temperature ranges correspond to subspinodal conditions for oceanic and continental fields. This suggests that no hydrothermal field can operate sustainedly in a superspinodal regime.

2.3.3. Cavitation

With boiling, cavitation is the other phenomenon associated to subspinodal liquid decompression, and is a two-step process. In a first step, fast liquid decompressions or high-speed liquid flows create transient and local density perturbations. The liquid pressure drops below the saturation pressure or even to negative values. As a result, the liquid is stretched up to a certain point until mechanical failure and apparition of microscopic cavities in the liquid [*Xiao and Heyes*, 2002]. Then, in a second step, the stretched liquid relaxes to equilibrium by elastic rebound. Thus, in the $P-T$ diagram of Figure 3, cavitation is represented by two vertical arrows: the first one, downward, indicates the liquid decompression up to the liquid metastable field, and the second one, upward, represents the compressive reaction towards the binodal curve. The vapour inside the cavities follows a similar pressure evolution, i.e. a pressure drop followed by a compression, but with some distinctive features. Firstly, the gas pressure remains always positive. Secondly, the compression leads the gas through the metastable field of supercooled gases, and then through the high-pressure unstable domain of steam. As a consequence, gas bubbles finish up to implode.

The implosion of these gas cavities is not without important consequences. The elastic rebound of the surrounding liquid produces a large amount of mechanical energy, which is focused on these microscopic imploding cavities. This process is similar to a stretched string, which hits the hanging wall and transfers to it a significant energy quantity. This

enormous concentration of energy is responsible of a localized and very fast increase of temperatures and pressures (up to 5000 K and 1000 bar [*Suslick et al.*, 1999]), followed immediately by a very rapid cooling. This is the development field of sonoluminescence [*Frenzel and Schultes*, 1934] and sonochemistry [*Caupin and Herbert*, 2006]. Additionally, cavitation allows to explain the formation of some natural geological, but exotic materials, like C_{60} and C_{70} fullerenes [*Phipps Morgan et al.*, 2004] or nanodiamonds [*Ozima and Tatsumoto*, 1997].

The close environment around collapsing cavities exerts also a strong influence on their dynamics. While the implosion of isolated bubbles can be approximated by a spherically symmetrical collapse [*Rayleigh*, 1917; *Benjamin and Ellis*, 1966; *Ohl et al.*, 1999], the dynamics of bubble implosions change drastically at the proximity or contact of a solid surface: the bubble surface is deformed by an involution, which gives rise to an energetic and high-speed liquid jet hitting the solid surface [*Ohl et al.*, 1999]. This phenomenon is similar to Taylor fluid instabilities caused by the collapse of steam films between boiling liquid and a hot surface, which are known to play an important role in water-magma interactions [*Wohletz*, 1986]: as a result, the magma is distorted up to the point to be torn out and fragmented into small bulbous, mossy and nearly spherical clasts, which are typically found in fluidal peperites [*Busby-Spera and White*, 1987].

Cavitation takes too an important part in superspinodal liquid decompressions. *Yu and Venart* [1996]; *Venart et al.* [2004]; *Abbasi and Abbasi* [2007] have demonstrated the existence of another type of explosive liquid decompressions, which have been called BLCBE (Boiling Liquid Compressed Bubble Explosion). These explosions are produced by the failure of a tank containing a pressurized liquid at near-critical conditions, but BLCBE

differs from BLEVE by the fact the container does not break off at once. Instead, in a first step, the container failure is limited to the development of a crack through which the depressurizing liquid escapes out. As a result, the initial depressurization wave in the vessel is followed by a reflected compression wave caused by the rapid expansion of the in-situ gas. The subsequent repressurization leads to coherent bubble collapse and cavitation. The implosion of the bubbles generates a shock wave, emitting a high dynamic pressure peak resulting to the final failure of the container. In this sense, BLCBE is a phenomenon relevant for describing the explosive liquid decompressions from hydrothermal reservoirs and magmatic chambers. In the same category of events, the rarefaction wave following a meteoritic impact [*Ozima and Tatsumoto*, 1997] or a deep-lithospheric eruption (the so-called "Verneshots" of *Phipps Morgan et al.* [2004]) are analoguous cavitation situations, where a depressurization is followed by a compressive requilibration. As a consequence, cavitation can be considered as one of the fundamental processes of volcanic and hydrothermal systems.

2.4. Expansion of a Gas Under Pressure

The sudden decompression of a pressurized gas is undoubtedly an explosive phenomenon, whose violence is sufficient to generate shock waves. However, at first sight, this explosion type does not seem to fit our theoretical framework proposed here, where explosions result from spinodal processes. Nevertheless, one can note that the equation of state of the perfect gas ($P\,v = R\,T$) predicts that the $(\partial\,P/\partial\,v)_T$ quantity tends to zero for high expansion degrees, indicating a begin of violation of the mechanical stability criterion (see equation 4). Moreover, the surface ($P = 0$) corresponds to a thermodynamic frontier in the $P - v - T$ space of the ideal gas, separating the forbidden domain of

negative pressures from the stable/metastable field of positive pressures. Thus, the limit ($P = 0$) of infinite expansion shares some similarity with the liquid spinodal boundary, as it generates also a violent explosion.

3. The Explosive Energy of Water

The mechanical energy released by any substance is function of its expansivity through the classical relation, valid under reversible conditions:

$$\mathrm{d}W = -P\,\mathrm{d}v, \tag{7}$$

where $\mathrm{d}W$ is the amount of mechanical energy produced by the expansion $\mathrm{d}v$ of a fluid. As a result, the main sources of explosive energy are: (1) the fluid exsolution from magma by magmatic vesiculation and/or fragmentation (*Burnham* [1979], (2) and the fluid expansion. Therefore, to quantify the energy balance of volcanism, it is necessary to differentiate precisely the explosive potential of the five energetic processes of water, which are respectively (1) liquid expansion by heating, (2) vaporization, (3) steam expansion by heating, (4) steam adiabatic decompression and (5) water exsolution from magma. We will see later that these contributions are, indeed, not involved in the same way for the different types of hydrothermal and magmatic systems. Thus, a close analysis of these different energetic sources is necessary. We have seen also that water metastability plays an important role in the explosive character of hydrothermal and volcanic eruptions. Hence, a last question to be addressed is how metastability modifies the energetic properties of water.

3.1. The Decompression Energy

Decompression up to the atmospheric pressure is the main source of mechanical energy produced by pressurized fluids. The eruption energy of hydrothermal systems (geysers) or volcanic systems comes principally from the opening and decompression of a deep fluid reservoir, which is suddenly connected to the atmosphere. It may even be proposed that this type of energy is produced during contact of lava with water under atmospheric pressure, as strong transient overpressures can be generated too by boiling of superheated waters [*Zimanowski et al.*, 1995].

The decompression process is so rapid that the system has not enough time to exchange heat with the exterior. Thus, to a first approximation, the decompression is considered to be adiabatic. A further simplification is to state that the decompression is reversible. This is clearly not exact (see below), but this allows to treat the decompression as an isentropic process (i.e., the entropy of the system is constant : $\mathrm{d}S = 0$).

3.1.1. Reversible Conditions

Using the Wagner and Pruss (2002) equation of state, the classic $T - U$ and $T - H$ diagrams (Figures 4 and 5) can be calculated to get a first estimation of the mechanical energy. They include isobaric and isentropic paths extrapolated up to the metastable fields. It can be noted that the isobars exhibit almost linear steep variations in $T-U$ and $T-H$ diagrams, except in the critical and metastable fields, where they depart from their general trends and tend to get horizontal. This behaviour can be explained by the specific properties of fluids in the spinodal and critical fields. Indeed, the slope of an isobar in a $T - U$ diagram is inversely proportional to the isochoric heat capacity:

$$\left(\frac{\partial T}{\partial U}\right)_P = \frac{1}{c_v} \tag{8}$$

In the same way, the slope of an isobar in a $T - H$ is inversely proportional to the isobaric heat capacity:

$$\left(\frac{\partial T}{\partial H}\right)_P = \frac{1}{c_P}. \tag{9}$$

Therefore, the horizontal slopes of isobars in $T - U$ and $T - H$ diagrams are caused by the divergence of isochoric and isobaric heat capacities at spinodal and critical points (e.g. [*Johnson and Norton*, 1991]). The reversible work released by an isentropic fluid expansion can be calculated from the first law of thermodynamics as a function of the internal energy:

$$\mathrm{d}U = T\mathrm{d}S - P\mathrm{d}V = -P\mathrm{d}V = \delta W_{\mathrm{rev}}. \tag{10}$$

The δW_{rev} quantity is conventionally counted as negative, as the system does a work on its surroundings, and so the mechanical work (W_U) is:

$$W_U = \Delta\, U = U_5 - U_3 < 0, \tag{11}$$

where (3) is the starting state of the decompression and (5) is the final state at atmospheric pressure. Equation 11 is valid for short-lived outbursts. For long-lasting eruptions or fluid flows, the enthalpy is more adapted to the calculation of the mechanical work (for example, the work yielded by a fluid flow in a vent above a magmatic chamber). As a result, the net mechanical work (W_H) of the venting fluid is:

$$\begin{aligned} W_H &= W_U + P_5\, v_5 - P_3\, v_3, \\ &= H_5 - H_3, \\ &= \Delta H \leq 0. \end{aligned} \tag{12}$$

where v stands here for the specific volume at the subscribed point.

The quantity W_H gives the amount of energy, which can be converted to gravitational potential energy (E_p), kinetic energy (E_c) and all other forms of mechanical energy (fragmentation, elastic deformation, shock waves, ...), noted E_d. Thus, the energetics of fluid flows and eruption phenomena can be assessed by using a modified form of Bernoulli's equation (Mastin, 1995):

$$-W_H = \Delta E_\mathrm{p} + \Delta E_\mathrm{c} + \Delta E_\mathrm{d} + {}'\text{frictional terms}'. \tag{13}$$

The last term of this equation takes into account frictions between fluid and the surroundings. Depending upon the importance of this frictional term, two contrasted cases can be considered: isenthalpic expansions and isentropic decompressions.

3.1.2. Isenthalpic Decompressions

The so-called isenthalpic fluid expansions are decompressions where all potential and kinetic energies are dissipated through frictions ($W_H = 0$). This situation occurs, in particular, for fluid flows in porous and tortuous media, such as aquifers. The evolution of these flows can be followed on a $T - H$ diagram (Figure 5) along a vertical line starting from the initial point (3). In most cases, isenthalpic decompressions are accompanied by a temperature decrease of the fluid (and a temperature increase of the surroundings). The

amplitude of this temperature decrease can be visualized by considering the offset between isobars drawn in Figure 5. Thus, this effect will be particularly marked for supercritical steams (T roughly between 400 and 700°C) and supercooled steams. This property is notably invoked to explain, in part, the heating of the surrounding rocks along pathways followed by steam flows (Armstead, 1978) in geothermal reservoirs.

3.1.3. Isentropic Decompressions

If the frictional term of equation 13 can be neglected, the expansion can be considered as a reversible isentropic process. To estimate graphically the mechanical work of decompression, isentropic expansion curves must be used. In Figures 4 and 5, several isentropic paths have been plotted. Detailed calculation examples are given for W_U and W_H in Table 3 by using equations 11 and 12. The corresponding paths (Figures 4 and 5) are composed of two parts:

1. a first part, at high pressures and temperatures, where the pressure drop runs in the monophasic field, between initial point (3) and point (4). Point (4) marks the demixing of a new fluid phase (liquid or gas). This fluid transition can be located either on the saturation curve (L(G) or G(L) binodal branch), or anywhere along the metastable extrapolation of the isentropic path up to a spinodal point.

2. the second part is the decompression in the biphasic liquid-gas domain, up to the atmospheric pressure (point 5).

To assess the energetic potential of a pressurized water reservoir, isentropic heat capacities $c_{U,S}$ or $c_{H,S}$ can be considered:

$$c_{U,S} = \left(\frac{\partial U}{\partial T}\right)_S, \tag{14}$$

$$c_{H,S} = \left(\frac{\partial H}{\partial T}\right)_S, \tag{15}$$

($c_{U,S}$ and $c_{H,S}$ coefficients are inversely proportional to the slope of isentropic paths, respectively in $T-U$ and $T-H$ diagrams). Isentropic decompression works W_U and W_S can be calculated from these parameters by:

$$W_U = \int_3^5 c_{U,S}\,\mathrm{d}T, \tag{16}$$

$$W_H = \int_3^5 c_{H,S}\,\mathrm{d}T. \tag{17}$$

As a result, energetic pressurized systems (for a given temperature difference between initial and final states) are characterized by elevated isentropic heat capacities. In Figures 4 and 5, it can be observed that most energetic isentropic paths are liquid-poor steams, featuring the lowest slope in $T-U$ and $T-H$ diagrams ($c_{H,S}$ well above 3 J/K). To the opposite, systems, which have a rather low isentropic heat capacity, are supercritical steams above 800–900 K ($c_{H,S}$ about 1 J/K) or liquid-rich biphasic liquid-gas mixtures ($c_{H,S}$ also around 1 J/K). By performing a study of the energy balance of isentropic decompressions of gas-liquid mixtures, similar to the one done by *Salla et al.* [2006] on isenthalpic expansions, it can be shown that there is a considerable energy transfer from the cooling liquid to the expanding steam. Therefore, the high energetic potential of wet steams is due to the condensation and cooling of liquid water droplets, providing an important energy source (up to 800 J/g of cooling liquid).

The relative contributions of monophasic and biphasic decompressions on the expansion work can be also analyzed in separate diagrams. Figure 6 displays the amplitude of the monophasic part $W_{U,1}$ of the mechanical work W_U in a $P-T$ diagram ($W_{U,1} = U_4 - U_3$). The monophasic decompression is especially important for hot and pressurized steams with $W_{U,1}$ values ranging from 200 to more than 1500 J/g. To the contrary, fluids of liquid-like densities have $W_{U,1}$ values below 100 J/g. The influence of the initial pressure on $W_{U,1}$ is negligible for a liquid. The intensity of the decompression work $W_{U,2}$ ($W_{U,2} = U_5 - U_4$) of a gas-liquid mixture is displayed in Figure 7 as a function of the saturation temperature. As stated above, this diagram confirms the high energetic potential of saturated steams. Maximum values of $W_{U,2}$ of 655 J/g are obtained for a steam starting to condense around 612 K (339°C). Coincidentally, this temperature is quite close to the superheat limit temperature ($T_{\rm sp}$ =593.6 K= 320.45°C) of water.

To take an example, steam, initially at a temperature of 1250 K (977°C) and a pressure of 1500 bar (in a reservoir at depth of 6 km), releases an energy W_U of 1000 J/g by decompression in the monophasic field (Figure 6). This energy amount is directly consumed to eject the fluid out of the erupting vent. From Figure 6, one reads that its saturation temperature is about 500 K (227°C). Therefore, the condensation will probably continue in the atmosphere, where the decompression in the biphasic domain will bring an additional energy quantity about 500 J/g. This energy source should play an important role in the dynamics of pyroclastic surges and flows. In conclusion, the steam expansion releases, theoretically, a total of 1500 J/g, a value which is to be compared with the explosive energy of gunpowder ($\simeq$ 2000 J/g) and TNT ($\simeq$ 4600 J/g). Thus, exsolved steam from a magmatic chamber can be doubtless classified as an explosive substance.

469 At this step, one question arises whether it is more appropriate to use isenthalpic or
470 isentropic conditions to assess the energetic intensity of an explosive process. In an isen-
471 thalpic process, all mechanical forms (gravitational, kinetic, ...) of energy are converted
472 to thermal energy, which is the fate of any depressurizing system after a certain amount
473 of time. Thus, the isenthalpic assumption is most adequate to characterize the fluid state
474 after complete relaxation. Conversely, in an isentropic process, the final state is fixed at
475 a virtual instant, where the system is charged with energy, but has not yet consumed it.
476 Thus, the isentropic assumption allows to calculate the amount of mechanical works.

477 **3.1.4. Ejecta**

478 To check the validity of the assessment of decompression works by our theoretical model,
479 one can attempt to compare it with volcanological observations by following an approach
480 developed by *Mastin* [1995]. For 1 kg of water interacting with a mass m_r of pyroclasts,
481 the Bernoulli's equation (equation 13) can be detailed to give the decompression work
482 W_H (in J/kg) as:

$$\begin{aligned} -W_H \;=\; & (1+m_r)\, g\, (z_5 - z_3) \\ & + \frac{1}{2}\,(1+m_r)\,(V_5^2 - V_3^2) \\ & + \text{'frictional terms'}, \end{aligned} \tag{18}$$

483 where V_3 and V_5 are the respective fluid velocities (in m/s) at points (3) and (5), g is
484 the gravity constant ($g = 9.81$ m^2/s), and z is the altitude. By taking the point (3) as
485 the reference altitude level (i.e. $z = 0$ for the magmatic chamber or the hydrothermal

reservoir), and by assuming that the fluid velocity V_3 is negligible before expansion, one obtains the general relation linking W_H to the height z and the fluid velocity V:

$$-W_H \simeq 10\,(1+m_r)\,z + 0.5\,(1+m_r)\,V^2 + \text{'frictional terms'}. \quad (19)$$

The last term of this equation, labeled 'frictional terms', includes all types of energy, which are difficult to characterize, i.e. fragmentation, ductile deformation, seismic energy, blasts .... To allow for this, the equation can be rewritten as:

$$-\zeta\,W_H \simeq 10\,(1+m_r)\,z + 0.5\,(1+m_r)\,V^2, \quad (20)$$

where ζ is a conversion factor of W_H into kinetic and gravitational energies, varying between 0 and 1. A value of 0.5 can be reasonably assumed for ζ. Thus, the maximum ballistic height $z_{\max}$ (in m) can be estimated by:

$$z_{\max} \simeq \frac{0.1}{(1+m_r)}\,\zeta\,|W_H|, \simeq \frac{0.1}{m_r}\,\zeta\,|W_H|, \quad (21)$$

or the maximal ejection speed (in m/s) by:

$$V_{\max} \simeq \sqrt{\frac{2\,\zeta\,|W_H|}{1+m_r}}, \simeq \sqrt{\frac{2\,\zeta\,|W_H|}{m_r}}, \quad (22)$$

or the mass m_r of pyroclasts (in kg) driven by the flow by:

$$m_r \simeq \frac{2\,\zeta\,|W_H|}{V_{\max}^2} - 1,$$

$$\simeq \frac{2\,\zeta\,|W_H|}{V_{\max}^2}. \quad (23)$$

Note that in all these equations 21-23, W_H must be expressed in J/kg of water.

Vulcanian eruptions are the best studied natural cases, and thus, allow us to compare observed data and model predictions. These eruptions are caused by the brittle failure of a lava dome overlying a pressurized gas zone, which formed either by exsolution of magmatic volatiles or rapid heating of groundwater [*Morissey and Mastin*, 2000]. Several eruptions (Arenal, Costa Rica, 1968; Ngauruhoe, New Zealand, 1975) have been the subject of measurements of ejection velocities of pyroclasts. The maximum velocities range between 200 and 400 m/s. By assuming a magma temperature between 1000 and 1200 K, the decompression work W_H of steam initially at pressures below 300 bar can be estimated from Figure 6 between 1100 and 1400 J/g of water. From equation 23 and with a value of 0.5 for ζ, the mass of pyroclasts driven by one kilogram of water can be calculated between 5.9 and 34 kilograms, i.e. a water weight fraction between 2.9 % and 14.5 % for the magma. The reversible assumption leads to somewhat overestimate the water content, although the lowest value is consistent with usual magmatic water contents.

3.1.5. Irreversible Conditions

Irreversibility can be taken into account by using the following general formula [*Planas-Cuchi et al.*, 2004], which calculates the final state at point (5) by decompression from point (3):

$$\begin{aligned} U_5 - U_3 &= -P_{\text{ext}}\,(v_5 - v_3), \\ &= -P_5\,(v_5 - v_3), \end{aligned} \tag{24}$$

where $P_{\text{ext}} = 1$ bar, and U is the molar internal energy. This equation is consistent with the following formulation of *Zhang* [2000] to allow for irreversibility in volcanic eruptions:

$$H_5 - H_3 = v_3\,(P_5 - P_3). \tag{25}$$

To solve equation 24, two distinct cases must be considered:

1. in the first case, the decompression leads to a stable monophasic system at point (5). The unknown is the value of the temperature T_5 with the constraint that the final temperature T_5 is above the normal boiling temperature ($T_5 > 373$ K). Thus, the process produces superheated steams (note here that the term "superheated" refers to a stable, and not metastable, state of a steam at temperatures above its saturation point, as it is the usage in the geothermics litterature). Therefore we have to numerically solve the equation:

$$U_5(T_5, v_5) - U_3 = -P_{\text{ext}}\,(v_5 - v_3). \tag{26}$$

where v_5 is the fluid molar volume at T_5 and 1 bar.

2. in the second case, the decompression leads to a stable biphasic liquid-gas association at $P_{\text{ext}} = 1$ bar and $T_5 = 373.15$ K. Equation 24 becomes:

$$f\,U_{\text{liq}} + (1 - f)\,U_{\text{vap}} - U_3 =$$

$$-P_{\text{ext}}\ \left[f\, v_{\text{liq}} + (1-f)\, v_{\text{vap}} - v_3\right], \tag{27}$$

where U_{liq} (J/mol), v_{liq} (m^3/mol), U_{vap} (J/mol) and v_{vap} (m^3/mol) are all calculated at 373.15 K and 1 bar. The unknown is the value f of the mass liquid fraction in the system and is simply calculated by:

$$f = \frac{P_{\text{ext}}\,(v_3 - v_{\text{vap}}) - U_{\text{vap}} + U_3}{U_{\text{liq}} - U_{\text{vap}} + P_{\text{ext}}\,(v_{\text{liq}} - v_{\text{vap}})}. \tag{28}$$

Results are given in Figure 8, which can be compared with Figure 6, where isocurves of the decompression energy and the mass liquid fraction at the final state have been plotted as a function of the initial pressure P_3 and temperature T_3. At initial atmospheric pressures (i.e. $P_3 = P_{\text{ext}}$), the decompression work is zero, whatever the steam temperature. For example, fumarolles have no explosive potential and cannot be exploited economically, except for heat. However, with increasing initial pressure P_3, the mechanical work, which can be extracted by expansion, increases drastically. As shown by the curvatures of the iso-W_U lines, there is an optimal pressure (from 31 bar at 700 K to 81 bar at 1200 K), at which the hot steam can release a maximum mechanical work for a given initial temperature T_3. At pressures higher than 300 bars, the fluid decompression becomes less energetic with increasing pressures, and the temperature becomes the key parameter controlling the mechanical energy content of the fluid.

It can be also observed (Figure 8) that the expansion under irreversible conditions produce final states, which are much more drier, as the result of the internal production of entropy by irreversibility.

But most importantly, it can be seen that the assumption of irreversible conditions leads to much smaller values for the decompression energy. Values range from 50 to 550 J/g of water, and represent around one fourth to one third of corresponding energies under reversible conditions. Up to now, reversibility has been almost always applied in the volcanological litterature [*Wohletz*, 1986; *Mastin*, 1995], with the notable exception of *Zhang* [2000], but irreversibility yields probably more realistic values of the explosive energy, even if it may be somewhat less practical to use. Indeed, the $T-U$ and $T-H$ diagrams cannot be used directly for the irreversible case, except if one uses the approximation of an isenthalpic process. In Figure 9, the mass liquid fraction of liquid-gas mixtures obtained by decompression up to 100°C and 1 bar of saturated liquid or steam is plotted as a function of the initial temperature for the three possible assumptions, i.e. isentropic, isenthalpic and irreversible cases. As expected, isenthalpic and irreversible depressurizations yield the most dry mixtures, and the isentropic expansion gives the highest liquid fraction. But, interestingly, it can be noted that the isenthalpic hypothesis provides a good approximation of the irreversible case, in particular for the liquid expansion. Thus, it is possible to rely on the isenthalpic decompression model to estimate the mass liquid fraction f of the final state at 100°C and 1 bar, by using the lever rule in the $T-H$ diagram of Figure 5. Then, the irreversible work (in J/g) of decompression of saturated liquid can be given by:

$$\begin{aligned} W_U &\simeq P_{\text{ext}} \left[(1-f)v_{\text{vap}} + f v_{\text{liq}} - v_3\right], \\ &\simeq P_{\text{ext}} \, (1-f) v_{\text{vap}}, \\ &\simeq 167 \, (1-f). \end{aligned} \tag{29}$$

563 This expression is accurate with a relative error, which is less than 1 % below 550 K,
564 and the maximum discrepancy does not exceed 4 % at the critical point.

3.2. The Vaporization Work

565 When cold water interacts with hot magma, the first event producing important me-
566 chanical work is vaporization. For one gram of boiling liquid water, the resulting energy
567 is given by:

$$W_{\text{vap}} = -P\,(v_{\text{vap}} - v_{\text{liq}})/M_{\text{H}_2\text{O}}, \tag{30}$$

568 where v_{vap} and v_{liq} are the molar volumes of saturated liquid and gas, and $M_{\text{H}_2\text{O}}$ is the
569 molar weight of water.

570 The amplitude of this energy is given in Figure 10 as a function of the boiling tempera-
571 ture. Its mean value is around 150 J/g, and it reaches a maximum at 495 K (222°C) and
572 24 bar, where almost 200 J/g can be yielded. This state corresponds to the point of max-
573 imum enthalpy of saturated steam. It is worth to observe that this maximum is obtained
574 at temperatures intermediate between normal boiling temperature and spinodal temper-
575 ature. Thus, the sudden boiling of superheated water at this temperature can give 20 %
576 more mechanical energy than normal boiling at 100°C. To the contrary, when approach-
577 ing near critical conditions, vaporization energy decreases considerably up to zero at the
578 critical point. It is also symptomatic to note that vapour-dominated geothermal systems,
579 such as Larderello (Italia) or The Geysers (California), have pressure-temperature condi-
580 tions which are close to the state of maximum enthalpy for saturated steams [*Goff and*
581 *Janik*, 2000].

3.3. The Heating Work

Fluids expand when they are heated. As such, they exert a mechanical work on their surroundings. Thus, water expansion by heating must be taken into account to assess the energetic balance of water explosions. The case of isobaric heating under reversible conditions will be considered here. In this case, the reversible work can be obtained from a simple difference of the enthalpy and the internal energy:

$$\mathrm{d}H - \mathrm{d}U = P\,\mathrm{d}v = -\delta W. \tag{31}$$

As the pressure is constant and is equal to the pressure of the surroundings ($P = P_{\mathrm{ext}}$), this equation is also valid under irreversible conditions. The variations of the isobaric heating work ($H - U$) is given in Figure 11 as a function of the temperature. Two contrasted behaviours can be observed. First, the heating work of liquids is practically negligible, as demonstrated by the vertical slopes of isobars. The heating of liquid in the metastable field delivers no mechanical work. To the opposite, steams can provide a significant contribution. Isobaric heating curves show a linear trend in the steam field. At low pressures ($P \leq 10$ bar), steam behaves as a perfect gas, and the isobaric expansion work is given by:

$$-W = \Delta(H - U) \simeq R\,\Delta T, \tag{32}$$

where R is the constant of ideal gas for water ($R = 8.31/18 = 0.4617$ J/g/K) and ΔT is the temperature increase. At higher pressures, the slopes of isobars decrease, indicating a higher mechanical energetic potential. For example, at 1000 bar, steam yields almost

599 twice as more expansion work than under atmospheric pressure for the same temperature
600 increase. Note also that the isobars in Figure 11 include the expansion work produced by
601 vaporization. Thus, as seen in the preceding section, one can recognize in Figure 11 the
602 peak of expansion work released by the vaporization of water at 222°C and 24 bar. Another
603 remarkable property of water is the very high potential of the mechanical expansion work
604 in the critical and the spinodal field of supercooled gases, as illustrated by the nearly
605 horizontal slopes of isobars.

606 To summarize, contact of cold liquid water with a hot body, like a basaltic flow, can
607 produce a mechanical work up to 600 J/g. As a result, vaporization and steam isobaric
608 heatings represent also significant energetic contributions of a water explosion.

3.4. The Exsolution Work

609 The exsolution work of water from magmas is another important source of energy, which
610 must be taken into account in magmatic systems. Indeed, the exsolution is accompanied
611 by a net volume increase from the partial molar volume $\overline{v}_{H_2O}$ of water to the molar volume
612 v of steam under the (P,T) exsolution conditions. Experimental data indicate that the
613 partial molar volume $\overline{v}_{H_2O}$ in hydrous silicate glasses is around 12 ± 0.5 cm^3/mol at room
614 temperature [*Richet et al.*, 2000; *Richet and Polian*, 1998]. With a partial molar thermal
615 expansion coefficient of H_2O about 4×10^{-5} [*Richet et al.*, 2000], a temperature increase
616 of 1000 K leads only to an augmentation of 4 % of $\overline{v}_{H_2O}$, i.e. 0.5 cm^3/mol. Inversely, a
617 pressure increase leads to a small decrease of $\overline{v}_{H_2O}$. Thus, we have retained a mean value
618 of 12 cm^3/mol for $\overline{v}_{H_2O}$ for the ranges of magmatic temperatures and pressures considered
619 here ($900\,\mathrm{K} < T < 1600\,\mathrm{K}$ and $1\,\mathrm{bar} < P < 3000\,\mathrm{bar}$).

To determine the exsolution work, the first idea would be to apply the same rigorous algorithms described in section 3.1.1 for a reversible process or section 3.1.5 for an irreversible one. However, no equation of state has been yet developed to describe the energetic properties of hydrous magmas, neither for its internal energy or its enthalpy. Thus, the trade-off is to focus only on the isothermal and isobaric exsolution work W_{ex} under the pressure-temperature conditions (P_3, T_3) in the magmatic chamber or at the fragmentation level in the volcanic conduit:

$$W_{\text{ex}} = -P_3 \, (v_{\text{vap}} - \overline{v}_{\text{H}_2\text{O}}), \tag{33}$$

where v_{vap} is the molar volume of steam calculated by the Wagner and Pruss equation of state [*Wagner and Pruss*, 2002] at (P_3, T_3) conditions. Values of the exsolution work are given in Figure 12. They range between 250 and 700 J/g of exsolved water. This represents a notable energetic contribution of magmatic systems (almost the double of the steam expansion work for a basaltic magma). The exsolution energies show rather a stronger dependence with respect to the temperature than to the pressure, except at pressures below 500 bar. The bulk explosion energy of a magmatic eruption is then estimated by the sum of W_{ex} and the expansion work W_U, calculated either under the reversible assumption (section 3.1.1, equation 11) or under the irreversible hypothesis (section 3.1.5, equation 24). For instance, a basaltic lava exsolving 1 weight percent of water at the earth surface produces only an exsolution energy of 5.5 J/g of magma at 1200 K (i.e. 550 J/g of water from Figure 12) and no steam expansion work at all (Figure 8). The same magma, exsolving in a magmatic chamber at a pressure of 500 bar generates 500 J/g of exsolved water and 420 J/g of water by irreversible decompression against the atmospheric

pressure, that is 920 J/g of water or 9.2 J/g of magma and per weight percent of exsolved water. Our model can also be applied to the 18 May 1980 eruption of the Mount St-Helens by using the parameters of *Zhang* [2000]: $T_3 = 1200$ K (927°C), $P_3 = 2200$ bar and a weight percent of exsolved water of 3.7 %. By assuming that the melt is entirely expelled by exsolving water, we estimate the mass of pyroclasts $m_r = (1000-37)/37 = 26$ kg for one kg of steam. From Figure 8, the irreversible decompression work is found to amount to 320 J/g of exsolved water, whereas from Figure 12, the exsolution work ranges between 420 J/g of exsolved water (exsolution at (P_3, T_3)) and 550 J/g of exsolved water (exsolution under the atmospheric pressure). This gives us a total mechanical work W between 740 and 870 J/g of exsolved water. From equation 22, we calculate a maximal ejection speed $V_{\max}$ between 165 m/s and 180 m/s by assuming an energy conversion factor ζ of 0.5. These values are in agreement with estimations of 100-110 m/s of the choked exit velocity [*Kieffer*, 1981] or with measurements of 150 m/s for the velocity of the lateral explosion cloud [*Friedman et al.*, 1981; *Voight*, 1981].

3.5. The Explosion Power

Up to now, we have discussed about the water explosivity in terms of energy quantities. However, what makes a good explosive is not the amount of work involved, but the production rate of work per time unit, in other words, its power or, equivalently, its yield expressed in mass of TNT. The explosivity of water is due to a physical transformation, the rate of which is a function of its metastability degree. The duration of explosive reactions between water and magma is on the order of the millisecond [*Zimanowski et al.*, 1991, 1995], thus an explosive vaporization of 500-1000 J/g represents a power of 500 kW

to 1 MW/g of water. The magnitude of this phenomenon is 3 to 4 orders higher than usual boiling conditions.

4. A Typology of Hydrothermal and Volcanic Systems

The preceding section have analyzed the different energetic contributions, i.e. fluid expansion accompanied or not by vaporization/condensation processes, isobaric boiling, and magmatic exsolution, and their explosive potentials have been discussed. A synthesis of their relative contributions in hydrothermal and volcanic systems can be done in a pressure-enthalpy diagram (Figure 13). The different cases are produced by the interactions in various proportions of (1) meteoric, superficial and connate waters, whose $P-T$ conditions are close to the mean geothermal gradient (left part), and (2) ascending magmas in the upper part of the crust, either intruding or extruding, (right part). Energy estimations given below are based on values calculated under the irreversibility assumption.

1. First, one can consider liquid-dominated geothermal systems, (A in Figure 13). The boiling must be triggered by a depressurization of the geothermal reservoir [*Armstead*, 1978]. Thus, the energy source comes mainly from the liquid boiling and steam expansion, well below 100 J/g of H_2O (see equation 29 and Figure 7). Moreover, their explosive potential is weak and is mainly represented by geysers (subspinodal decompressions).

2. Next (B in Figure 13), these are supercritical or slightly subcritical fluids, typically found in the lithocaps of magmatic chambers [*Norton and Dutrow*, 2001], or in deep geothermal systems (black smokers of oceanic ridges). Sudden pressure drops on such systems up to atmospheric conditions are expected to lead to superspinodal decompressions and produce explosions of high power (for instance, see the isentropic decompression

curve labeled 700 K, which intersects the liquid spinodal curve in Figure 13). Such events would involve a mechanical energy of 150–200 J/g of H_2O (Figure 8).

3. Then, vapour-dominated geothermal systems (C in Figure 13) produce mechanical energy by expansion of gaseous fluids, below 150 J/g of H_2O (Figure 7). Well-known examples include the geothermal fields of Larderello (Italia) or The Geysers (California). The deep parts and the porous spaces of these geothermal fields contain saturated waters in larger proportions than steam [*Goff and Janik*, 2000]. Steam migrates upwards in the fractures by isenthalpic boiling, but the condensing liquid separates and percolates deeper. As a consequence, steam evolves progressively towards the state of maximum enthalpy.

4. In the field labeled D are found fluids exsolved by magmas during their cooling and crystallization in a magmatic chamber, a few kilometers below the surface. These are volatile-rich magmas, as well as hot and pressurized fluids. The mechanical energy of of vulcanian and plinian volcanisms is produced by magmatic exsolution (450–600 J/g of H_2O) and steam expansion (from 200 J/g to 400 J/g of H_2O, Figure 8).

5. And finally, liquid waters (E) which are suddenly heated by contact with hot magmatic lavas at Earth surface. This includes surtseyan volcanism and superficial phreato-magmatism. The mechanical work is mainly produced by heating, and amounts to levels between 200 and 600 J/g of H_2O (Figure 11). Moreover, explosive boiling of water can create transient overpressures, probably of several ten bars [*Zimanowski et al.*, 1995]. Thus, the irreversible decompression of these fluids will give an additional energy amount between 100-300 J/g (Figure 8).

Note that the bulk energy released by phreato-magmatism can be as high as in plinian volcanism. However, a correct assessment of the energy of a phreato-magmatic explosion

requires a global analysis of the energy balance, as carried out by *Wohletz* [1986], that is based on the determination of the interactive water–magma mass ratio.

5. Geophysical Application: Estimation of Volcanic Impacts

In the same way than the thermodynamic models of *Wohletz* [1986, 2002] and *Mastin* [1995], our model can be applied to case studies of volcanic and hydrothermal eruptions. Volcanic impacts can be approximated from a few number of scaling laws, using the explosion yield, expressed in tons of TNT. For instance, it is possible to estimate the overpressure of the blast [*Kingery and Pannill*, 1964; *Taniguchi and Suzuki-Kamata*, 1993], the diameter of the crater [*Nordyke*, 1962; *Wohletz and Heiken*, 1992; *Goto et al.*, 2001] or the height of the explosion cloud [*Ohba et al.*, 2002]. These similarity rules are mostly based on a cubic root formulation:

$$R = R_0 \, W^{1/3}, \tag{34}$$

where R is the distance from the explosion center, at which an event of given intensity is observed; R_0 is a scaling parameter and W is the explosion energy. The scaling parameter R_0 is usually derived from correlations established from impact studies of explosions of energy W_0 (either chemical explosives [*Van den Berg and Lannoy*, 1993] or nuclear bombs). In general, these methods must be used with caution [*Browne and Lawless*, 2001], and, in particular, their application must take care of specified validity conditions (explosive type, site geometry, confinement, explosion depth and others ...).

One application example can be made on the study of *Ohba et al.* [2007] about a small phreatic eruption on the flank of a dacite lava dome of Akita Yakeyama, northern Honshu, Japan, which occured in 1997 and lasted for 70 minutes. The source of eruption was a

hot aquifer, situated at about 1000 m of depth at a temperature ca. 300–350°C and a pressure between 110 and 240 bar. The explosions were triggered by initial mud effusions from the overlying plumbing system, which released the pressure in the deep reservoir. Therefore, the explosions extract their energy from the boiling and steam expansion. The bulk volume of muddy materials involved in the eruption was estimated around 1000 m^3 with an initial water contents of 18–20 wt.%, a rock density of 2400 kg/m^3 and a water density between 580 and 720 kg/m^3. From these parameters, we can estimate the mass of explosive liquid water between 300 and 320 tons. From Figure 7, the explosion energy can be estimated between 242 and 370 J/g of H_2O under the classical reversibility hypothesis, and between 68 and 93 J/g of H_2O by assuming irreversibility. This yields a bulk explosive work between 72 and 120 GJ for a reversible process, which is somewhat below the estimations of *Ohba et al.* [2007] between 100 and 200 GJ by using the method of *Mastin* [1995]. The irreversibility hypothesis gives an estimate between 20 and 28 GJ. *Ohba et al.* [2007] used also similarity rules to estimate the energy of discrete explosions from the size of one of the craters [*Nordyke*, 1962; *Goto et al.*, 2001] and from the height of the observed clouds [*Ohba et al.*, 2002]. The energy of the largest explosions was estimated between 3 and 5 GJ by *Ohba et al.* [2007]. Thus, our estimates of the bulk explosive energy remain consistent with the similarity models used by *Ohba et al.* [2007]. Figure 8 can also be used to evaluate the mass of vapour produced by the eruption. One obtains mass fractions of steam, between 32 and 41 weight % for an isentropic process, and between 41 and 54 weight % for an irreversible one. Both estimates are coherent with the muddiness of air-fall deposits. From Figure 13, one can note that the aquifer of the Akita Yakeyama volcano is just near or inside the shaded area of the explosive field of the $H - P$ diagram.

This fact is well confirmed by the explosive nature of this hydrothermal system, which contrasts markedly from geothermal ones of lower temperatures. As noted by *Ohba et al.* [2007], the craters are produced by the shallow explosions of the ascending and bubbling muds at depths of 6-10 m, corresponding to near atmospheric pressures ca 1–2 bar. By referring to the $P - T$ diagram of Figure 4, it can be noticed that the irreversible and adiabatic (and nearly isothermal) decompression path of these fluids at initial 300–350°C runs near the liquid spinodal curve Sp(L) at these surficial levels. Hence, it is suggested to associate the explosion focus to a "spinodal" zone, where the metastable bubbly muds reequilibrate violently by intensive spontaneous bubble nucleations and expansions. This conclusion could be well justified by the muddy nature of these fluids, featuring probably important concentration gradients and high viscosities, which delay their reequilibration with respect to external changes. In the classification of *Zhang* [2000], such a system tends to a "dynamically completely irreversible" behaviour, which is the trademark of explosive systems.

6. Conclusion

Rapid physical transformations (mainly magma exsolution, steam decompression or heating) are the causes of strong water instabilities, which lead to the explosive manifestations featured by hydrothermal and magmatic systems. These explosive properties of water have been treated here from a macroscopic point of view by using basic and fundamental concepts (yet rarely used in the volcanological litterature), such as metastability and spinodals. This approach can be fruitful to predict the explosive character of a transformation, here based on an one-component perspective. As a result, this allows us to differentiate superspinodal transformations, which are highly explosive (e.g. BLEVE),

and subspinodal ones, which are non or moderately explosive (e.g. cavitation or geysering). The adopted phenomenological point of view can be linked to the more common kinetic approach, as the physical mechanism of equilibrium relaxation differ also between metastable systems (nucleation-growth process) and unstable ones (spinodal decomposition).

The specific energetic properties of water have been presented both in the metastable and stable domains with the help of the Wagner and Pruss equation of state [*Wagner and Pruss*, 2002]. The mechanical work of the different possible physical transformations, including decompression, boiling, isobaric heating and magma exsolution has been assessed both under the reversibility and irreversibility assumptions. Up to now, the reversibility hypothesis has been almost always used for quantifying the energy balance of eruptions. Here is proposed a pathway to do calculations under the irreversible assumption which results in more realistic estimates. Then, a classification of the hydrothermal and volcanic systems has been proposed by taking into account their energetic balance and their explosivity. Finally, we show how the model can be used in conjunction with empirical scaling laws to predict potential impacts of volcanic eruptions.

Acknowledgments. This work has received financial support from the ANR (Agence Nationale de la Recherche) for the project SURCHAUF-JC05-48942. Professors Michel Pichavant, Bruno Scaillet, Ariel Provost, and Alain Burgisser are gratefully thanked for a first review of the manuscript. We are also grateful to Didier Laporte and Nicolas Cluzel for their help on magma properties. We have also appreciated the valuable comments from Prof. Y. Zhang, an anonymous reviewer and the Associated Editor. The calculation

786 programs used in this work can be found at the following address: `http://wwwobs.`

787 `univ-bpclermont.fr/lmv/pperm/thiery_r/index.html`.

References

Abbasi, T., and S. Abbasi (2007), The boiling liquid expanding vapour explosion (BLEVE): Mechanism, consequence assessment, management, *Journal of Hazardous Materials*, *141*, 480–519, doi:10.1016/j.jhazmat.2006.09.056.

Armstead, H. (1978), *Geothermal energy, its past, present and future contributions to the energy needs of man.*, Spon Ltd, London.

Benjamin, T., and A. Ellis (1966), XX. The collapse of cavitation bubbles and the pressures thereby produced against solid boundaries, *Phil. Trans. R. Soc. Lond. A*, *260*, 221–240.

Birk, A., and M. Cunningham (1996), Liquid temperature stratification and its effect on BLEVEs and their hazards, *Journal of Hazardous Material*, *48*, 219.

Browne, P., and J. Lawless (2001), Characteristics of hydrothermal eruptions, with examples from New Zealand and elsewhere, *Earth-Science Reviews*, *52*, 299–331.

Burnham, C. (1979), Magmas and hydrothermal fluids, in *Geochemistry of hydrothermal ore deposits*, edited by H. Barnes, pp. 71–136, Wiley, New York.

Busby-Spera, C., and J. White (1987), Variation in peperite textures associated with differing host-sediment properties, *Bull. Volcanol.*, *49*, 765–775.

Casal, J., and J. Salla (2006), Using liquid superheating for a quick estimation of overpressure in BLEVEs and similar explosions, *Journal of Hazardous Materials*, *A137*, 1321–1327, doi:10.1016/j/jhazmat.2006.05.001.

Caupin, F., and E. Herbert (2006), Cavitation in water: a review, *C. R. Physique*, *7*, 1000–1017.

Debenedetti, P. (1996), *Metastable Liquids*, 411 pp., Princeton University Press, Princeton, New Jersey.

Debenedetti, P. (2000), Phase separation by nucleation and by spinodal decomposition: Fundamentals, in *Supercritical Fluids: Fundamentals and Applications*, edited by K. Kiran, P. Debenedetti, and C. Peters, Nato Science Series E, pp. 123–166, Kluwer Academic Publishers, Dordrecht/The Netherlands.

Frenzel, H., and H. Schultes (1934), Luminescenz in ultraschallbeschickten Wasser, *Z. Phys. Chem.*, *27b*, 421–424.

Friedman, J., G. Oehloeft, G. Johnson, and D. Frank (1981), Heat content and thermal energy of the June dacitic dome in relation to total energy yield, May-October 1980, in *The 1980 Eruptions of Mount St. Helens*, *U.S. Geol. Surv. Prof. Paper*, vol. 1250, edited by P. Lipman and D. Mullineaux, pp. 557–567, Washington, U.S.

Goff, F., and C. Janik (2000), Geothermal systems, in *Encyclopedia of volcanoes*, pp. 817–834, Academic Press.

Goto, A., H. Taniguchi, M. Yoshida, T. Ohba, and H. Oshima (2001), Effects of explosion energy and depth to the formation of blast wave and crater: field explosion experiment for the understanding of volcanic explosions, *Geophys. Res. Lett.*, *28*, 4287–4290.

Imre, A., K. Martinas, and L. Rebelo (1998), Thermodynamics of negative pressures in liquids, *J. Non-Equilib. Thermodyn.*, *23*(4), 351–375.

Johnson, J., and D. Norton (1991), Critical phenomena in hydrothermal systems: state, thermodynamic, electrostatic, and transport properties of H_2O in the critical region, *American Journal of Science*, *291*, 541–648.

Kieffer, S. (1981), Fluid dynamics of the May 18, 1980 blast at Mount St Helens, in *The 1980 Eruptions of Mount St. Helens*, *U.S. Geol. Surv. Prof. Paper*, vol. 1250, edited by P. Lipman and D. Mullineaux, pp. 379–401, Washington, U.S.

Kingery, C., and B. Pannill (1964), Peak over-pressure vs scaled distance for TNT surface burst, *Tech. Rep. 1518*, Aberdeen.

Kiselev, S. (1999), Kinetic boundary of metastable states in superheated and stretched liquids, *Physica A*, *269*, 252–268.

Kiselev, S., and J. Ely (2001), Curvature effect on the physical boundary of metastable states in liquids, *Physica A*, *299*, 357–370.

Kokelaar, B. (1986), The mechanism of surtseyan volcanism, *J. Geol. Soc. London*, *140*, 933–944.

Lasaga, A. (1998), *Kinetic Theory in the Earth Sciences*, Princeton, New Jersey, 811 pp., Princeton University Press.

Lee, K. (2001), Classification of geothermal resources by exergy, *Geothermics*, *30*, 431–442.

Leidenfrost, J. (1756), On the fixation of water in diverse fire. Duisburg. In German; trans. Wares C. 1966., *International Journal of Heat and Mass Transfer*, *9*, 1153–1166.

Mastin, L. (1995), Thermodynamics of gas and steam-blast eruptions, *Bull. Volcanol.*, *57*, 85–98.

Mills, A. (1984), Pillow lavas and the Leidenfrost effect, *J. Geol. Soc. London*, *141*, 183–186.

Mills, M. (2000), Volcanic aerosol and global atmospheric effects, in *Encyclopedia of volcanoes*, edited by H. Sigurdson, Academic Press.

Morissey, M., and L. Mastin (2000), Vulcanian eruptions, in *Encyclopedia of volcanoes*, pp. 463–475, Academic Press.

Moyer, T., and D. Swanson (1987), Secondary hydroeruptions in pyroclastic-flow deposits: examples from Mount St Helens, *J. Volcanol. Geotherm. Res.*, *32*, 299–319.

Nonnenmacher, T. (1980), On the kinetics of spinodal decomposition, *Z. Physik B – Condensed Matter*, *38*, 327–333.

Nordyke, M. (1962), An analysis of cratering data from desert alluvium, *J. Geophys. Res.*, *67*, 1965–1974.

Norton, D., and B. Dutrow (2001), Complex behaviour of magma-hydrothermal processes: role of supercritical fluid, *Geochim. Cosmochim. Acta*, *65*(21), 4009–4017.

Ohba, T., H. Taniguchi, H. Oshima, M. Yoshida, and A. Goto (2002), Effect of explosion energy and depth on the nature of explosion cloud – a field experimental study., *J. Volcanol. Geotherm. Res.*, *115*, 33–42.

Ohba, T., H. Taniguchi, T. Miyamoto, S. Hayashi, and T. Hasenaka (2007), Mud plumbing system of an isolated phreatic eruption at Akita Yakeyama volcano, northern Honshu, Japan, *J. Volcanol. Geotherm. Res.*, *161*, 35–46.

Ohl, C.-D., T. Kurz, R. Geisler, O. Lindau, and W. Lauterborn (1999), Bubble dynamics, shock waves and sonoluminescence, *Phil. Trans. R. Soc. Lond. A*, *357*, 269–294.

Ozima, M., and M. Tatsumoto (1997), Radiation-induced diamond crystallization: origin of carbonados and its implications on meteorite nano-diamonds, *Geochim. Cosmochim. Acta*, *61*(2), 369–376.

Phipps Morgan, J., T. Reston, and C. Ranero (2004), Contemporaneous mass extinctions, continental flood basalts, and 'impact signals': are mantle plume-induced lithospheric

gas explosions the causal link ?, *Earth and Planetary Science Letters*, *217*, 263–284, doi:10.1016/S0012-821X(03)00602-2.

Planas-Cuchi, E., J. Salla, and J. Casal (2004), Calculating overpressure from BLEVE explosions, *Journal of Loss Prevention in the Process Industries*, *17*, 431–436, doi:10.1016/j.jlp.2004.08.002.

Rayleigh, L. (1917), On the pressure developed in a liquid during the collapse of a spherical cavity, *Phil. Mag.*, *34*, 94–98.

Reid, R. (1983), Rapid phase transitions from liquid to vapor, *Advances in Chemical Engineering*, *12*, 105–208.

Richet, P., and A. Polian (1998), Water as a dense icelike component in silicate glasses, *Science*, *281*, 396–398.

Richet, P., A. Whittington, F. Holtz, H. Behrens, S. Ohlhorst, and M. Wilke (2000), Water and the density of silicate glasses, *Contrib. Mineral. Petrol.*, *138*, 337–347.

Salla, J., M. Demichela, and J. Casal (2006), BLEVE: a new approach to the superheat limit temperature, *Journal of Loss Prevention in the Process Industries*, *19*, 690–700, doi:10.1016/j.jlp.2006.04.004.

Shmulovich, K., L. Mercury, R. Thiéry, C. Ramboz, and M. El Mekki (2009), Experimental superheating of pure water and aqueous solutions, *Geochim. Cosmochim. Acta*, *(accepted)*.

Sparks, R. (1978), The dynamics of bubble formation and growth in magmas: a review and analysis, *J. Volcanol. Geotherm. Res.*, *3*, 1–37.

Spieler, O., B. Kennedy, U. Kueppers, D. Dingwell, B. Scheu, and J. Taddeuci (2004), The fragmentation threshold of pyroclastic rocks, *Earth and Planetary Science Letters*,

226, 139–148, doi:10.1016/j.epsl.2004.07.016.

Suslick, K., Y. Didenko, M. Fang, T. Hyeon, K. Kolbeck, W. McNamara, M. Mdleleni, and M. Wong (1999), Acoustic cavitation and its chemical consequences, *Phil. Trans. R. Soc. Lond. A*, *357*, 335–353.

Taniguchi, H., and K. Suzuki-Kamata (1993), Direct measurement of overpressure of a volcanic blast on the June 1991 eruption at Unzen volcano, Japan, *Geophys. Res. Lett.*, *20*(2), 89–92.

Theofanous, T. (1995), The study of steam explosions in nuclear systems, *Nuclear Engineering and Design*, *155*, 1–26.

Thiéry, R. (1996), A new object-oriented library for calculating high-order multivariable derivatives and thermodynamic properties of fluids with equations of state, *Computers & Geosciences*, *22*(7), 801–815.

Thomas, N., C. Jaupart, and S. Vergniolle (1994), On the vesicularity of pumice, *J. Geophys. Res.*, *99*, 15,633–15,644.

Van den Berg, A., and A. Lannoy (1993), Methods for vapour cloud explosion blast modeling, *Journal of Hazardous Materials*, pp. 151–171.

Venart, J., G. Rutledge, K. Sumathipala, and K. Sollows (2004), To BLEVE or not to BLEVE: anatomy of a boiling liquid expanding vapor explosion, *Process Safety Progress*, *12(2)*, 67–70.

Voight, B. (1981), Time scale for the first moments of the May 18 eruption, in *The 1980 Eruptions of Mount St. Helens*, *U.S. Geol. Surv. Prof. Paper*, vol. 1250, edited by P. Lipman and D. Mullineaux, pp. 69–86, Washington, U.S.

Wagner, W., and A. Pruss (2002), The IAPWS formulation 1995 for the thermodynamic properties of ordinary water substance for general and scientific use, *J. Phys. Chem. Ref. Data*, *31*, 387–535.

Wohletz, K. (1983), Mechanisms of hydrovolcanic pyroclast formation: Grain-size, scanning electron microscopy, and experimental studies, *J. Volcanol. Geotherm. Res.*, *17*(1–4), 31–63.

Wohletz, K. (1986), Explosive magma-water interactions: thermodynamics, explosion mechanisms, and field studies, *Bull. Volcanol.*, *48*, 245–264.

Wohletz, K. (2002), Water/magma interaction: some theory and experiments on peperite formation, *J. Volcanol. Geotherm. Res.*, *114*, 19–35.

Wohletz, K., and H. Heiken (1992), *Volcanology and Geothermal Energy*, 432 pp., Univer. California Press.

Wohletz, K., T. McGetchin, M. S. II, and E. Jones (1984), Hydrodynamic aspects of caldera-forming eruptions: numerical models, *J. Geophys. Res.*, *89*(B10), 8269–8285.

Xiao, C., and D. Heyes (2002), Cavitation in stretched liquids, *Proc. R. Soc. Lond. A*, *458*, 889–910.

Yu, C., and J. Venart (1996), The boiling liquid collapsed bubble explosion (BLCBE): a preliminary model, *Journal of Hazardous Materials*, *46*, 197–213.

Zhang, Y. (1999), A criterion for the fragmentation of bubbly magma based on the brittle failure theory, *Nature*, *402*, 648–650.

Zhang, Y. (2000), Energetics of gas-driven limnic and volcanic eruptions, *J. Volcanol. Geotherm. Res.*, *97*, 215–231.

943 Zhang, Y., B. Sturtevant, and E. Stolper (1997), Dynamics of gas-driven eruptions: exper-
944 imental simulations using CO_2-H_2O-polymer system, *J. Geophys. Res.*, *102*, 3077–3096.
945 Zheng, Q. (1991), Liquids under tension and glasses under stress, Ph.D. thesis, Purdue
946 University, West Lafayette, Ind.
947 Zheng, Q., D. Durben, G. Wolf, and C. Angell (1991), Liquids at large negative pressures:
948 water at the homogeneous nucleation limit, *Science*, *254*, 829.
949 Zimanowski, B., V. Lorenz, and G. Fröhlich (1986), Experiments on phreatomagmatic
950 explosions with silicate and carbonatitic melts, *J. Volcanol. Geotherm. Res.*, *30*, 149–
951 155.
952 Zimanowski, B., G. Fröhlich, and V. Lorenz (1991), Quantitative experiments on
953 phreatomagmatic explosions, *J. Volcanol. Geotherm. Res.*, *48*(3–4), 341–358.
954 Zimanowski, B., G. Fröhlich, and V. Lorenz (1995), Experiments on steam explosion by
955 interaction of water with silicate melts, *Nuclear Engineering and Design,*, *155*, 335–343.
956 Zimanowski, B., R. Büttner, and V. Lorenz (1997a), Premixing of magma and water in
957 MFCI experiments, *Bull. Volcanol.*, *58*, 491–495.
958 Zimanowski, B., R. Büttner, V. Lorenz, and H.-G. Häfele (1997b), Fragmentation of
959 basaltic melt in the course of explosive volcanism, *J. Geophys. Res.*, *102*, 803–814.

Figure 1. Water volume fraction (f_v) in a mixture of melt, crystals and water as a function of the pressure P and temperature T, and for a water mass fraction of 5 % (A) and 15 % (B). A value of 2500 kg/m^3 has been chosen for the density of the melt and solids. The density of water is calculated with the equation of state of *Wagner and Pruss* [2002]). Lines are iso-f_v curves. In figure A, the corresponding density of the aqueous phase is indicated between parentheses in kg/m^3.

Figure 2. The stable, metastable and unstable fields of water projected in the $T-v$ space. The full lines separating the stable and metastable regions are the binodal curves: the first branch, noted L(G), refers to the saturated liquid water; whereas the other one, noted G(L), refers to the saturated steam. Both branchs join to the critical point (noted CP). The dashed curves are the two spinodal curves, which start from the critical point and delimit the unstable field from the metastable region. The first one, noted Sp(L), is the liquid spinodal curve; and the second one, noted Sp(G), is the gas spinodal curve.

Figure 3. $P-T$ diagram illustrating the different processes generating fluid instability. Solid line: the saturation curve (Sat.). Dotted lines: the liquid spinodal curve (Sp(L)) and the gas spinodal curve (Sp(G)). These three curves meet at the critical point (CP).

Figure 4. $T - U$ diagram used for estimating the mechanical work produced by isentropic expansions. This diagram includes several types of curves: (1) isobars (full thin lines), calculated at 1, 10, 50, 100, 200, 300 500 and 1000 bar; (2) isentropic decompression curves (dashed lines) for a monophasic system; and (3) isentropic decompression curves (dashed lines) for a biphasic system. Isentropic curves are labeled by their temperature at 1000 bar. Other elements of the diagram are the binodals (thick solid lines) L(G) and G(L); and the spinodals (dotted curves) Sp(L) and Sp(G).

Figure 5. $T - H$ diagram used for estimating isobaric heat transfer and mechanical work produced by isenthalpic or isentropic fluid circulations. This diagram includes several types of curves: (1) isobars (full thin lines), calculated at 1, 10, 50, 100, 200, 300, 500 and 1000 bar; (2) isentropic decompression curves (dashed lines) for a monophasic system; and (3) isentropic decompression curves (dashed lines) for a biphasic system. Isentropic curves are labeled by their temperature at 1000 bar. Other elements of the diagram are the binodals (thick solid lines) L(G) and G(L); and the spinodals (dotted curves) Sp(L) and Sp(G).

Figure 6. $P - T$ diagram showing the mechanical energy released by the reversible isentropic expansion of hot steam (in J/g of water) as a function of the initial pressure P and temperature T in the magmatic chamber. Thick solid lines: total work ($W_U = U_3 - U_5$) produced in the monophasic and biphasic fields. Thick dashed lines: mechanical work ($W_U = U_3 - U_4$) produced in the monophasic region. Dotted lines: isotherms of the condensation temperature (in K) of the steam at 1 bar. Below the isotherm 373 K, both curves of monophasic and total works are coincident.

Figure 7. The expansion work (J/g of water) of a liquid-gas mixture against atmospheric pressure as a function of the initial saturation temperature. The full line indicates energies calculated for an isentropic decompression process, whereas the dashed curve is calculated for an irreversible adiabatic expansion. L(G), G(L) and CP represent respectively expansion works calculated for a saturated liquid, a saturated steam and a critical fluid.

Figure 8. $P - T$ diagram showing the mechanical work (full solid lines, in J/g of water) released by the irreversible adiabatic expansion of hot and pressurized steam as a function of the initial $P - T$ conditions. Dashed lines indicate the liquid fraction (in mass percentage) of the gas-liquid mixture at a final state of 1 bar and 100°C. The field to the right of the 0% curve indicates the generation of superheated steams at 1 bar (i.e. with a final temperature above 100°C).

Figure 9. The mass liquid fraction of the liquid-gas mixture at 100°C and 1 bar produced by the depressurization of a saturated liquid (full curve) or saturated steam (dashed curve), as calculated by three types of decompression processes, i.e. isentropic, isenthalpic and irreversible expansions.

Figure 10. The mechanical work (in J/g of water) produced by liquid vaporization, as a function of the boiling temperature.

Figure 11. $T - W$ diagram to calculate the work ($W = H - U$, in J/g of water) produced by fluid isobaric expansion as a function of the initial and final temperatures. For example, to calculate the expansion work done by heating the fluid from point A (T_A = 694 K) to point point B (T_B = 975 K) at constant pressure (here 1 bar), one makes the difference $W_B - W_A$ (= 450 − 320 = 130 J/g). Dotted lines are projections of the spinodal curves Sp(L) and Sp(G). Full thick lines are projections of the binodal curves L(G) and G(L). Thin solid lines are the isobars calculated at pressures of 1, 10, 50, 100, 200, 300, 500 and 1000 bar.

Figure 12. $P-T$ diagram showing the work produced by the isobaric and isothermal exsolution of water from magma (in J/g of exsolved water) at fixed pressure P and temperature T.

Figure 13. $P - H$ diagram. Thick solid curves: binodal L(G) and G(L) curves. Thick dotted curves: spinodal Sp(L) and Sp(G) curves. Thin dashed curves: isotherms calculated at T = 200, 300, 350, 374 (critical isotherm), 390, 500, 750, 1000 and 1227°C. Thin solid lines: isentropic expansion curves labeled by the initial fluid temperatures at 1000 bar. Majuscule letters refer respectively to: A: Liquid-dominated geothermal systems of low enthalpy. B: High-pressure hydrothermal systems of medium enthalpy. C: Vapour-dominated geothermal systems of high enthalpy. D: Exsolved magmatic, hot and pressurized, steams of vulcanian and plinian volcanic systems. E: Hot and low-pressure steams produced by superficial phreato-magmatism.

Table 1. List of symbols.

Symbol	Description
T	temperature
P	pressure
v	molar volume, m^3/mol
A	Helmholtz free energy
H	enthalpy
U	internal energy
S	entropy
W	mechanical work
ρ	density (kg/m^3)
M_{H_2O}	molar weight of water, 0.018 kg/mol
f	mass (or molar) liquid fraction in a biphasic liquid-gas mixture
f_v	volume liquid fraction in a biphasic liquid-gas mixture
T_i, P_i	initial temperature and pressure
T_f, P_f	final temperature and pressure
T_c	water critical temperature, 374°C, 647.096 K
T_{sat}	saturation temperature, 100°C, 373.15 K at 1 bar
T_{sp}	liquid spinodal temperature at 1 bar, 320.45°C , 593.6 K
T_{hn}	spontaneous homogeneous nucleation temperature, 304°C, 577 K at 1 bar
T_L	Leidenfrost temperature
c_v, c_P	isochoric and isobaric heat capacity, J/kg/K
ζ	conversion factor of the mechanical energy into kinetic and potential energy ($0 \leq \zeta \leq 1$)
$c_{U,S}$, $c_{H,S}$	isentropic heat capacities, J/kg/K
m_r	pyroclasts mass driven by one kg of water
V	flow velocity of ejected water and pyroclasts, m/s
$\overline{v}_{H_2O}$	partial molar volume of H_2O in silicate melts

Table 2. Comparative summary of the two fundamental kinetics, nucleation-growth and spinodal decomposition, of first-order phase transitions for an initial fluid. Note that the explosivity property is relevant only for the boiling of a liquid.

Main Characteristics		Nucleation-Growth	Spinodal Decomposition
Starting state		Metastable	Unstable
Process nature		Activated	Spontaneous
Initial density fluctuations			
	Localisation	At nucleation sites	Everywhere
	Amplitude	High	Low
	Wavelength	Short	Long
Final spatial biphasic pattern		Well separated liquid and gas	Imbricated biphasic association
Reactive zone		Boiling front	Everywhere
Mean diffusion length of heat and/or mass transfer		Large	Small
Transformation rate		Low to high	Very high
Explosivity		Low to high	Very high

Table 3. Calculation example of the mechanical energy released by a fluid isentropic decompression (*: calculated on the gas branch of the saturation curve), either in the case of a transient process, or a flow process.

State	Transient Process	Flow Process
Point 3 (900 K, 1000 bar)	$U_3 = 2711$ J/g	$H_3 = 3003$ J/g
Point 4* (615 K, 149 bar)	$U_4 = 2465$ J/g	$H_4 = 2615$ J/g
Point 5 (373.15 K, 1 bar)	$U_5 = 1799$ J/g	$H_5 = 1911$ J/g
% of liquid at point 5	34 %	34 %
Mechanical energy	$W_U = 912$ J/g	$W_H = 1092$ J/g

Table 4. Classification of the different hydrothermal and volcanic system types as a function of their nature, environment, energy source, energy amplitude, and explosivity. [1]: these values are calculated by assuming an equal contribution of (1) magma exsolution and decompression, and (2) liquid boiling and steam heating.

Type	Fluid nature	Environment	Energy source	Energy (J/g H_2O)	Explosivity
A	Liquid	Liquid-dominated geothermal systems	Decompression	0–100	Weak
B	Super-critical	Deep hydrothermal systems	Decompression	150–200	Low to high
C	Steam	Vapour-dominated geothermal systems	Decompression	100–150	Weak
D	Steam	Vulcanian and Plinian volcanism	Exsolution and decompression TOTAL	450–600 200–400 650–1000	High
E	Liquid	Surtseyan volcanism, superficial phreato-magmatism	Boiling and decompression TOTAL[1]	200–600 100–300 150–450	High
E+D	Liquid and steam	Phreato-plinian volcanism	Exsolution, decompression and boiling TOTAL[1]	450–600 200–400 200–600 425–800	Very high

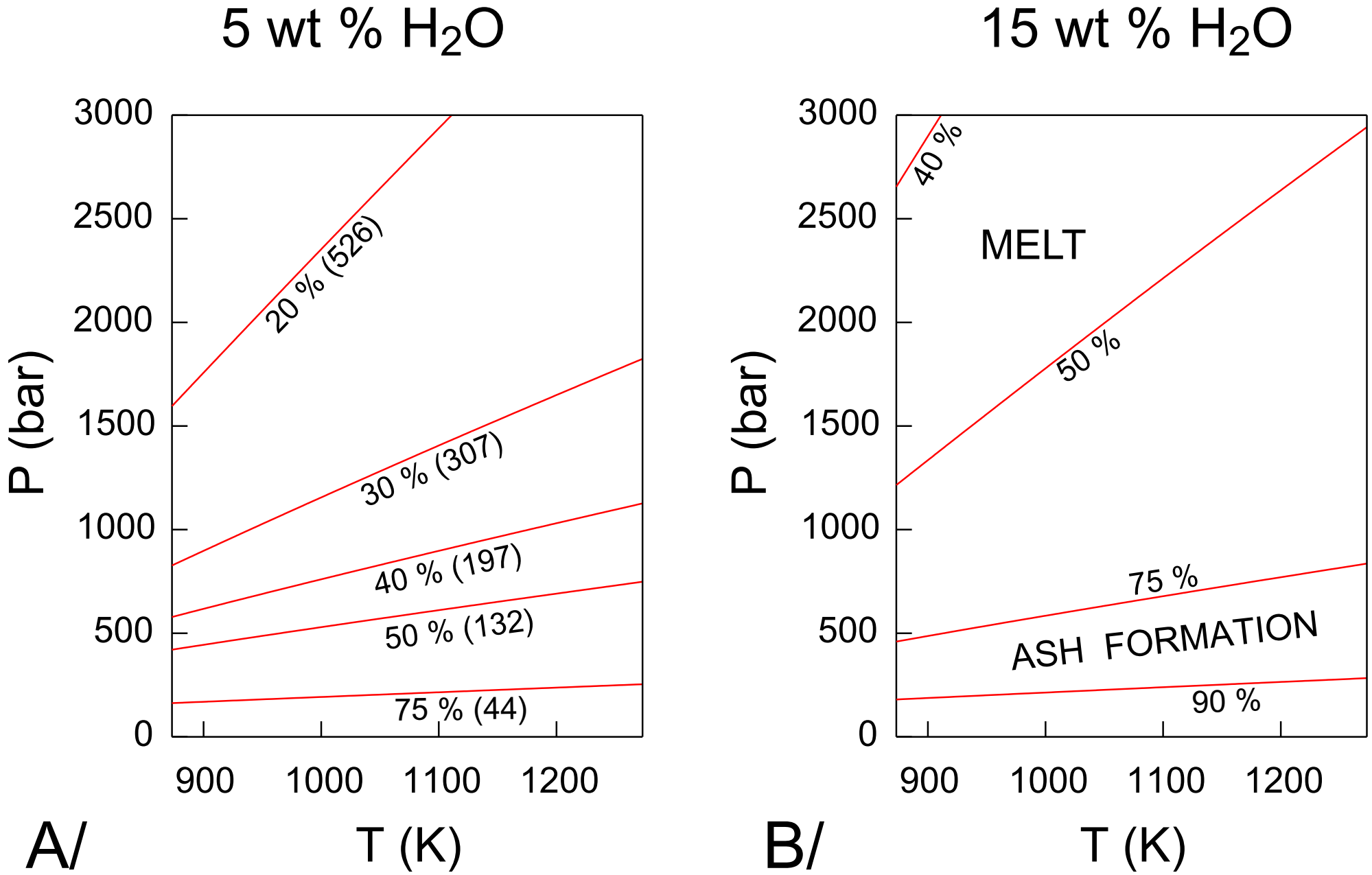
5 wt % H2O
15 wt % H2O
P (bar)
T (K)
3000
2500
2000
1500
1000
500
0
900
1000
1100
1200
20 % (526)
30 % (307)
40 % (197)
50 % (132)
75 % (44)
40 %
50 %
75 %
90 %
MELT
ASH FORMATION
A/
B/

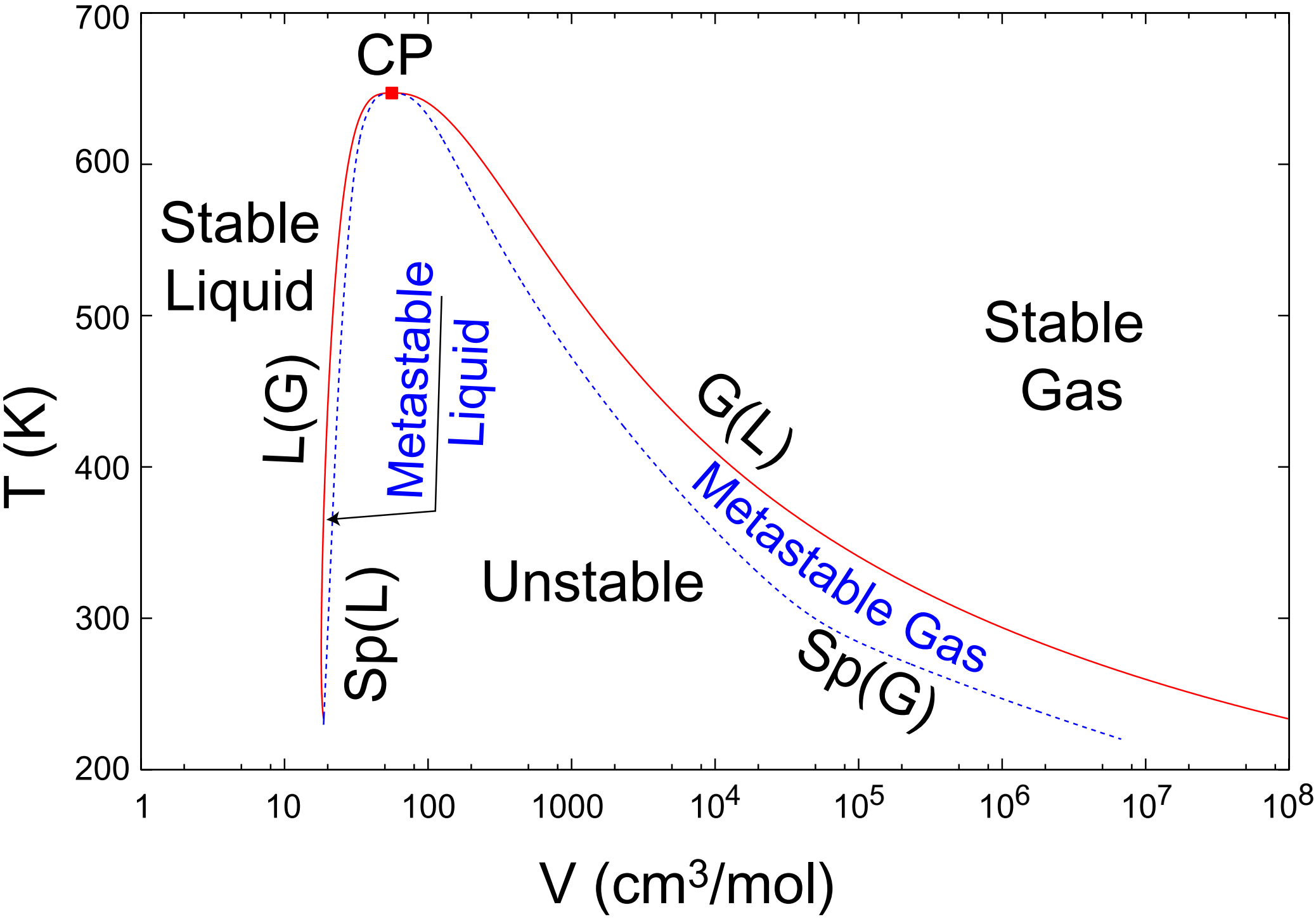
CP
Stable
Liquid
Stable
Gas
Unstable
L(G)
Metastable
Liquid
G(L)
Metastable Gas
Sp(L)
Sp(G)
T (K)
V (cm3/mol)
700
600
500
400
300
200
1
10
100
1000
10^4
10^5
10^6
10^7
10^8

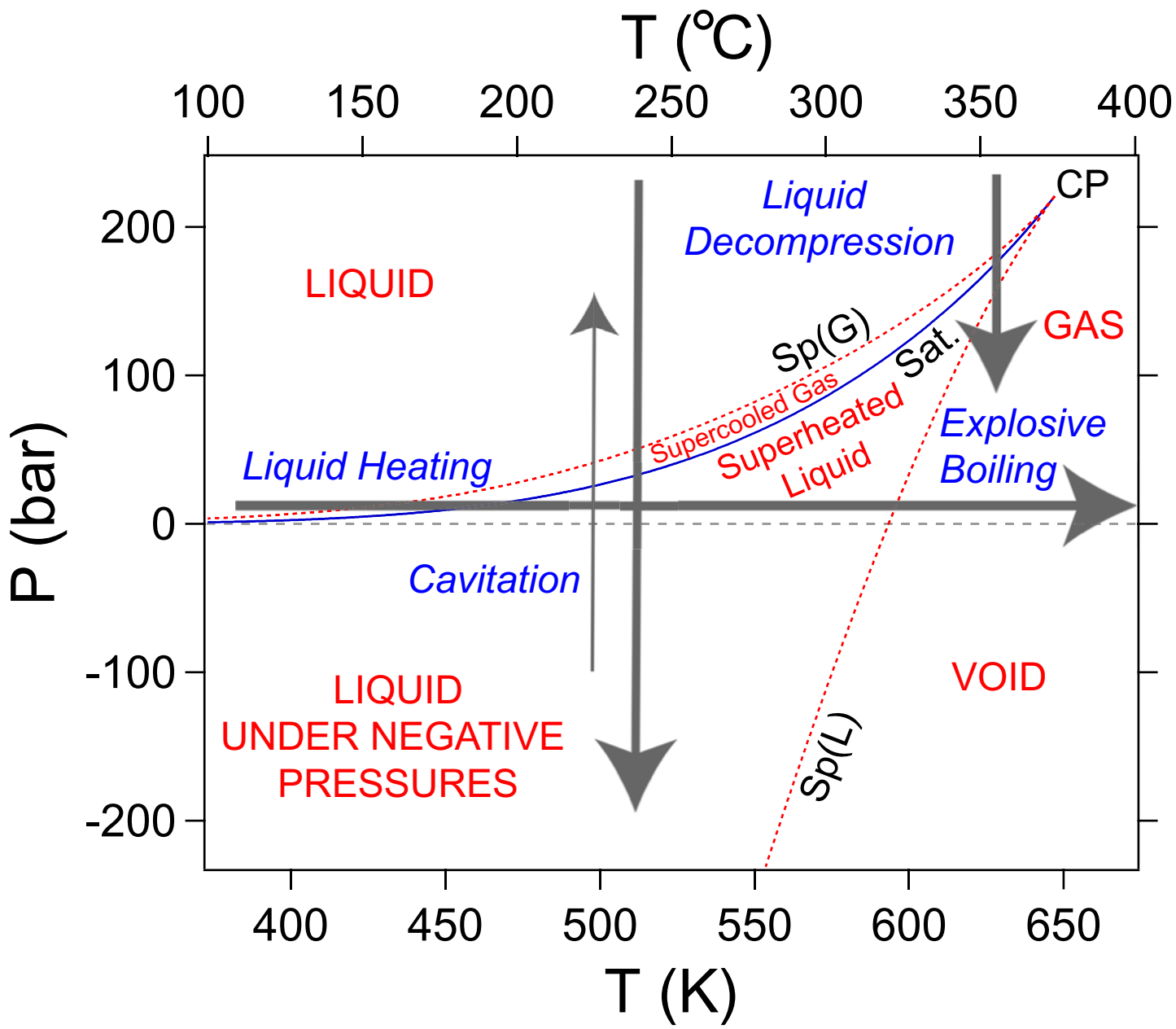
T (°C)
100
150
200
250
300
350
400
200
100
0
-100
-200
P (bar)
LIQUID
Liquid
Decompression
CP
GAS
Sp(G)
Sat.
Supercooled Gas
Superheated
Liquid
Explosive
Boiling
Liquid Heating
Cavitation
LIQUID
UNDER NEGATIVE
PRESSURES
VOID
Sp(L)
400
450
500
550
600
650
T (K)

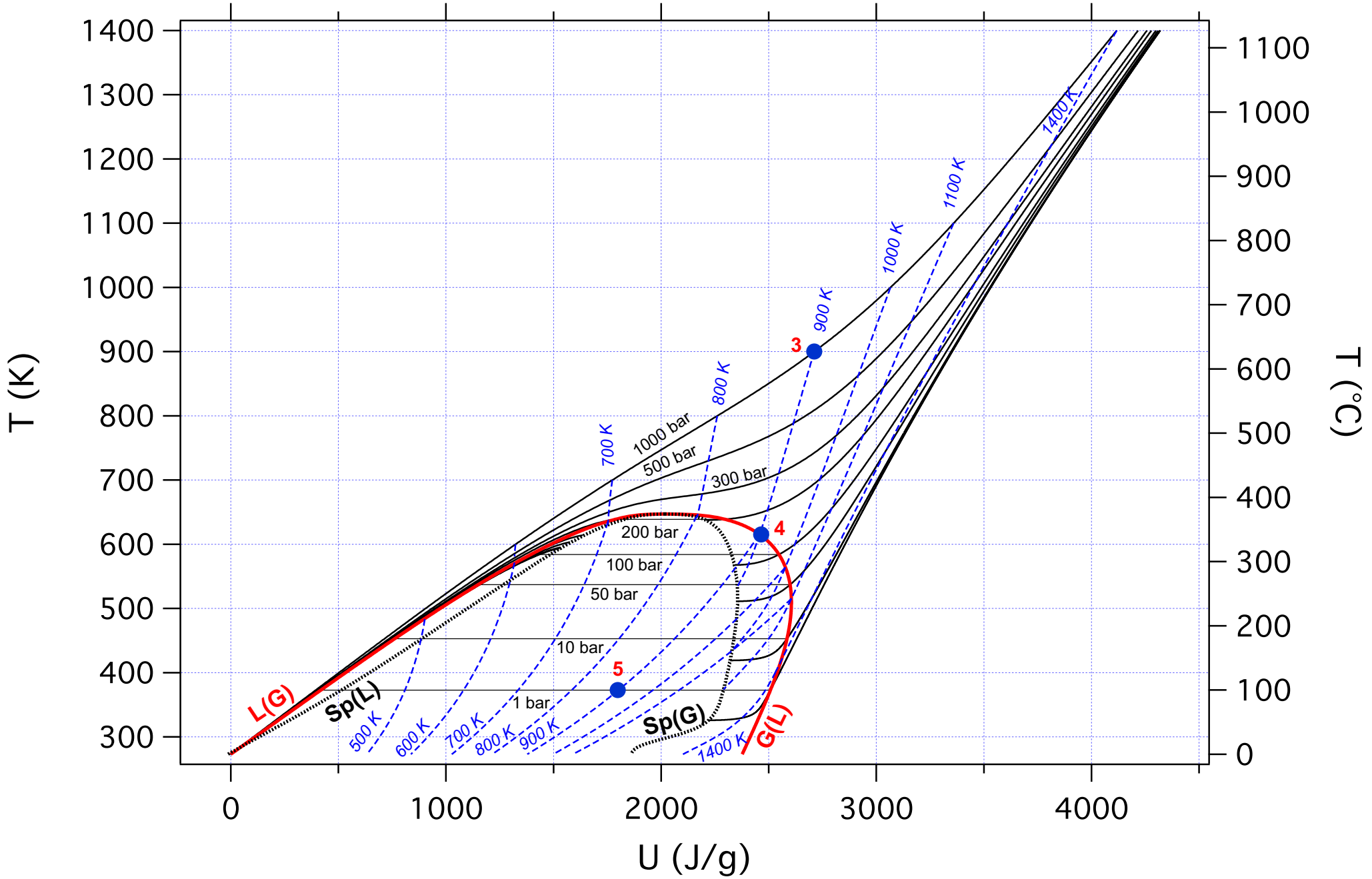
T (K)
T (°C)
U (J/g)
1400
1300
1200
1100
1000
900
800
700
600
500
400
300
1100
1000
900
800
700
600
500
400
300
200
100
0
0
1000
2000
3000
4000
L(G)
Sp(L)
Sp(G)
G(L)
3
4
5
1000 bar
500 bar
300 bar
200 bar
100 bar
50 bar
10 bar
1 bar
700 K
800 K
900 K
1000 K
1100 K
1400 K
500 K
600 K
700 K
800 K
900 K
1400 K

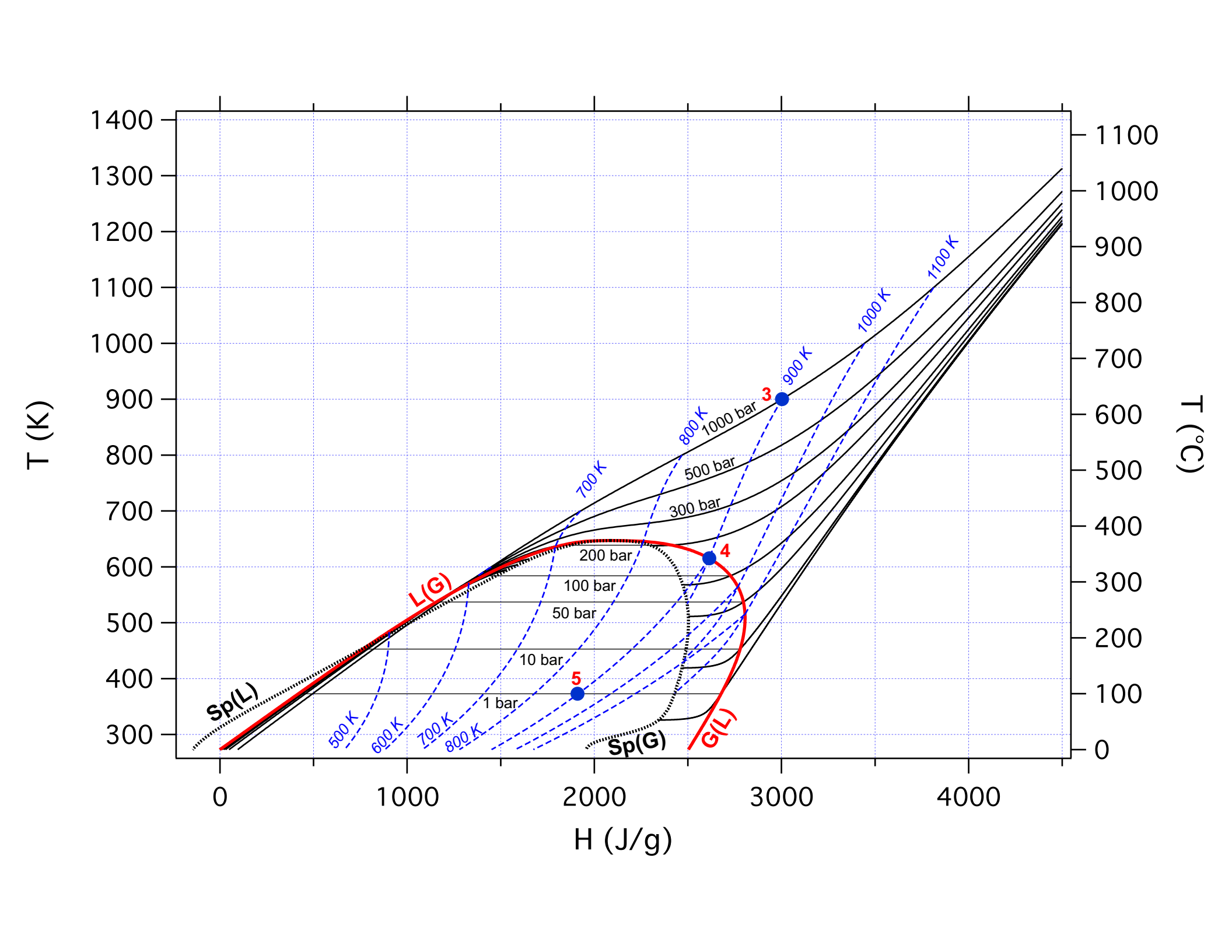
T (K)
T (°C)
H (J/g)
1400
1300
1200
1100
1000
900
800
700
600
500
400
300
1100
1000
900
800
700
600
500
400
300
200
100
0
0
1000
2000
3000
4000
1000 bar
500 bar
300 bar
200 bar
100 bar
50 bar
10 bar
1 bar
500 K
600 K
700 K
800 K
900 K
1000 K
1100 K
L(G)
G(L)
Sp(L)
Sp(G)
3
4
5

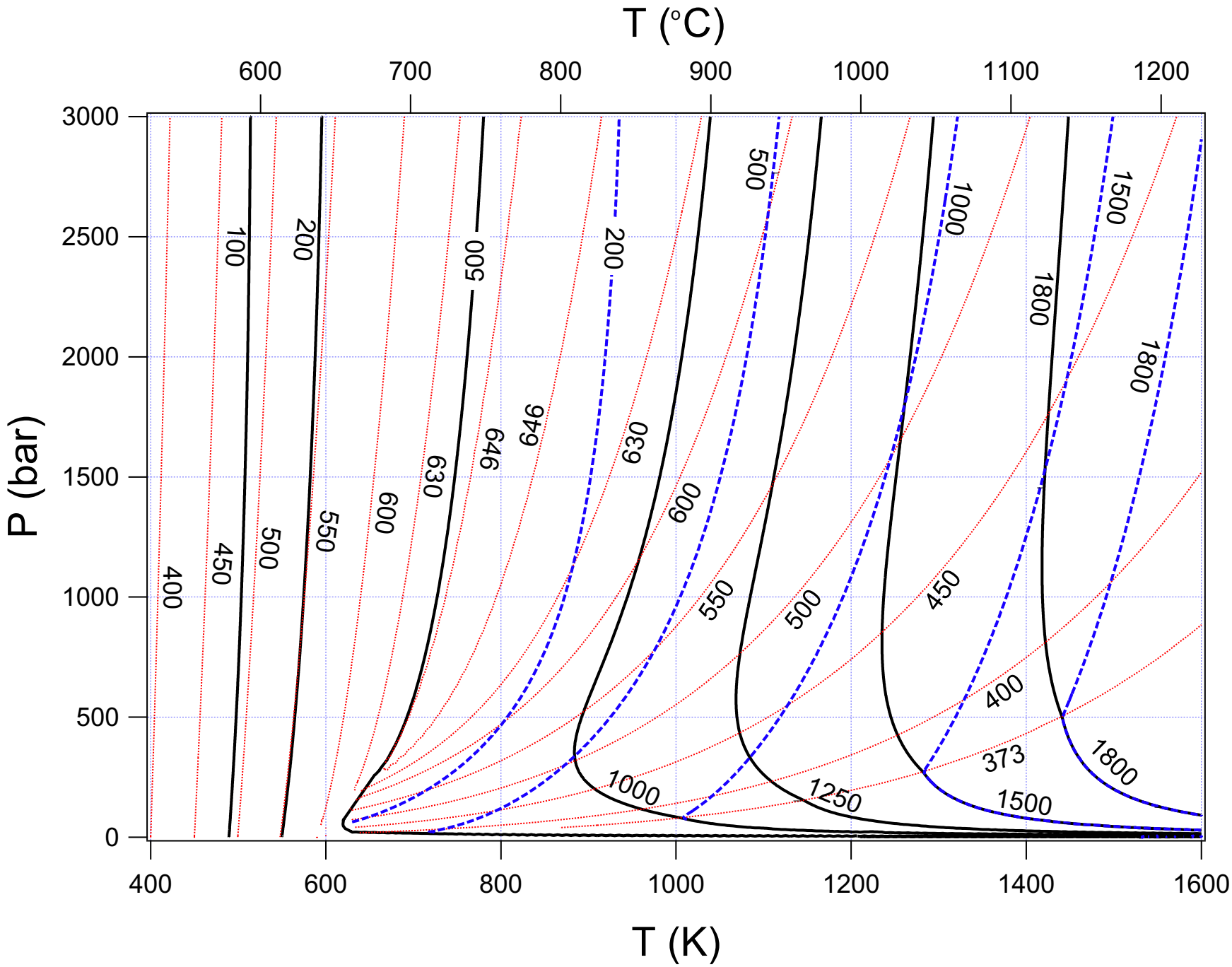
T (°C)
600
700
800
900
1000
1100
1200
P (bar)
3000
2500
2000
1500
1000
500
0
400
600
800
1000
1200
1400
1600
T (K)
100
200
500
646
630
600
550
500
450
400
200
500
630
646
600
550
500
450
400
373
1000
1250
1500
1800
500
1000
1500
1800
1800

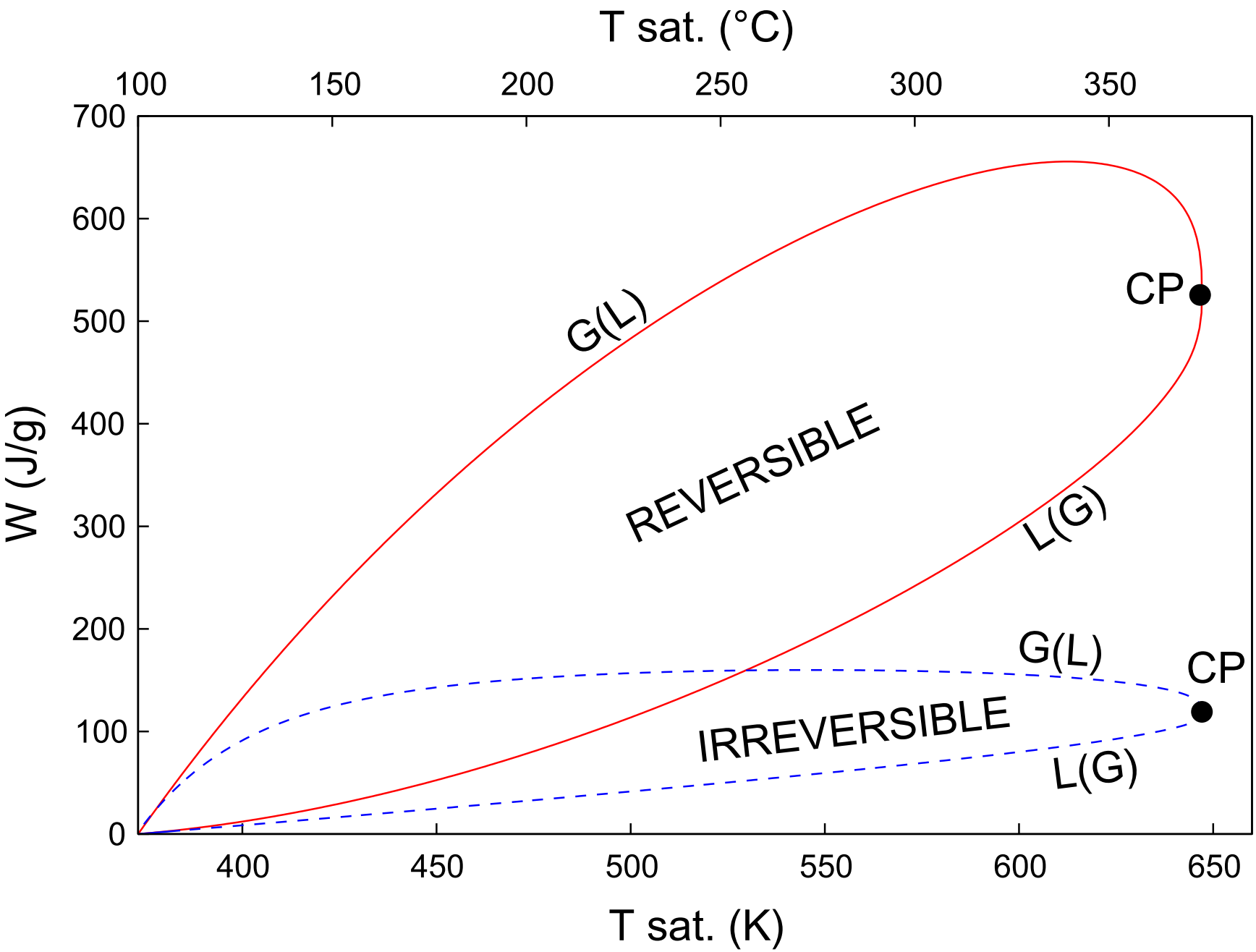
T sat. (°C)
100
150
200
250
300
350
700
600
500
400
300
200
100
0
W (J/g)
G(L)
REVERSIBLE
L(G)
CP
G(L)
IRREVERSIBLE
L(G)
CP
400
450
500
550
600
650
T sat. (K)

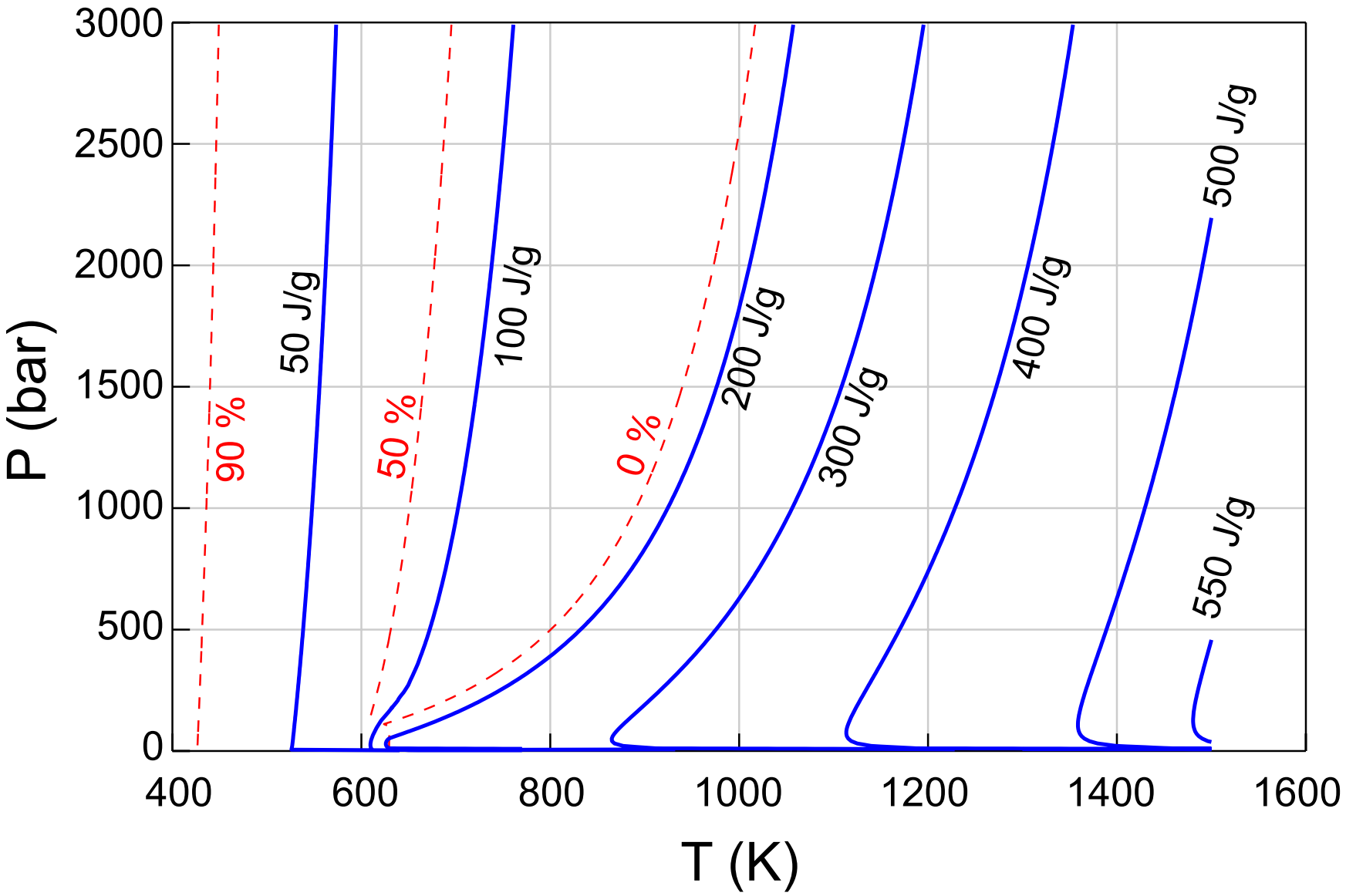
P (bar)
T (K)
3000
2500
2000
1500
1000
500
0
400
600
800
1000
1200
1400
1600
90 %
50 %
0 %
50 J/g
100 J/g
200 J/g
300 J/g
400 J/g
500 J/g
550 J/g

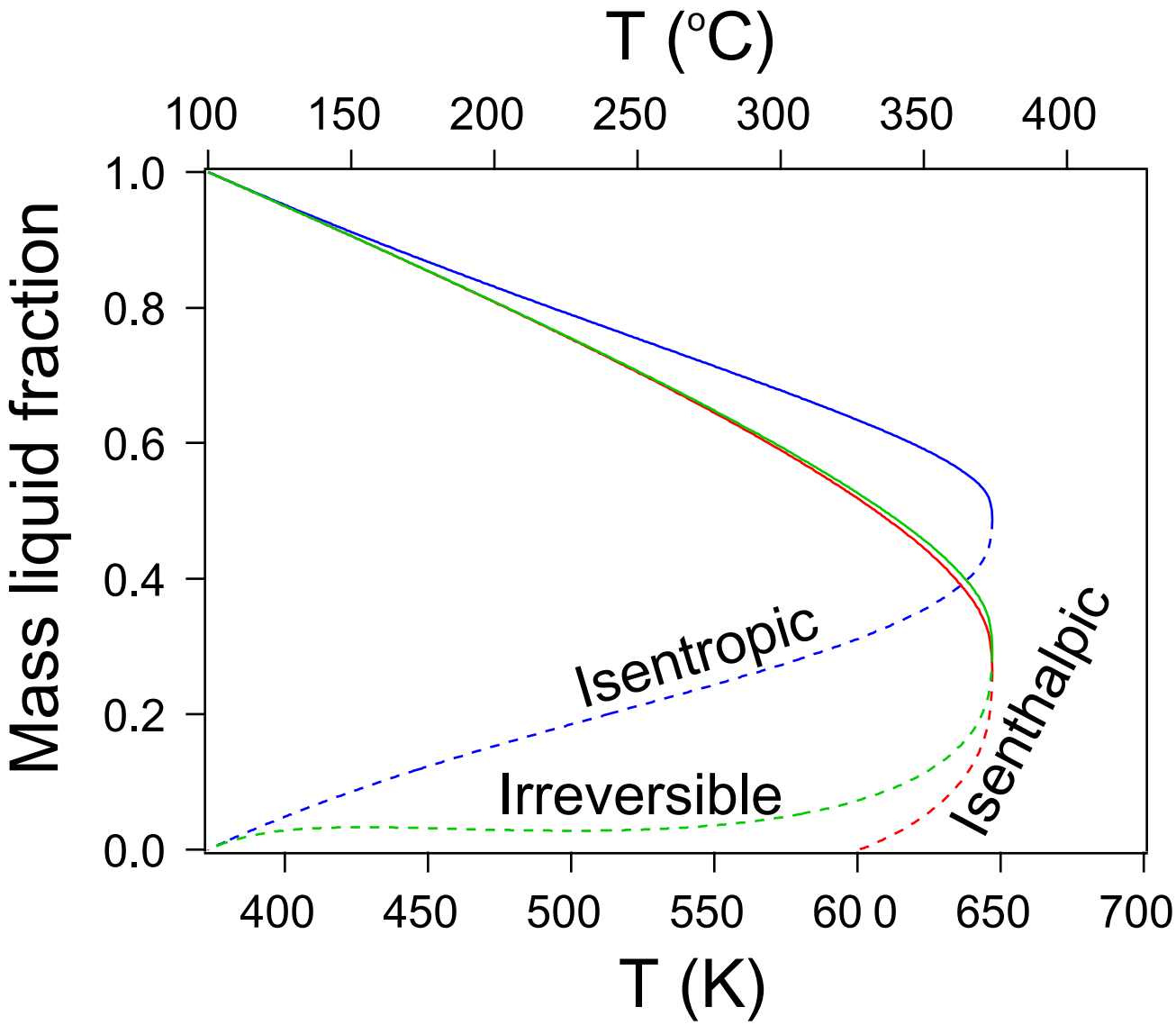
T (°C)
100
150
200
250
300
350
400
Mass liquid fraction
1.0
0.8
0.6
0.4
0.2
0.0
Isentropic
Irreversible
Isenthalpic
400
450
500
550
60 0
650
700
T (K)

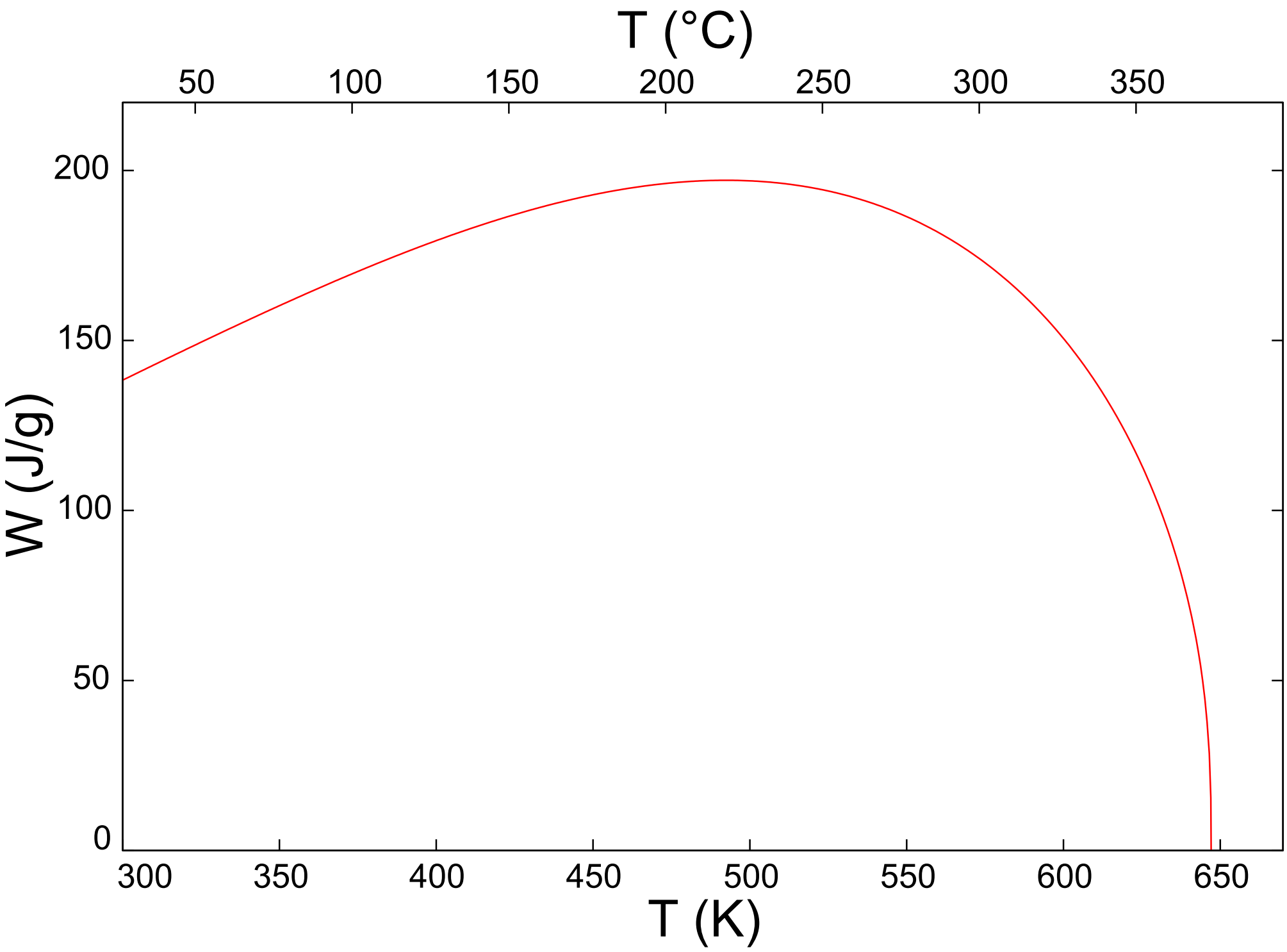
T (°C)
50
100
150
200
250
300
350
W (J/g)
200
150
100
50
0
300
350
400
450
500
550
600
650
T (K)

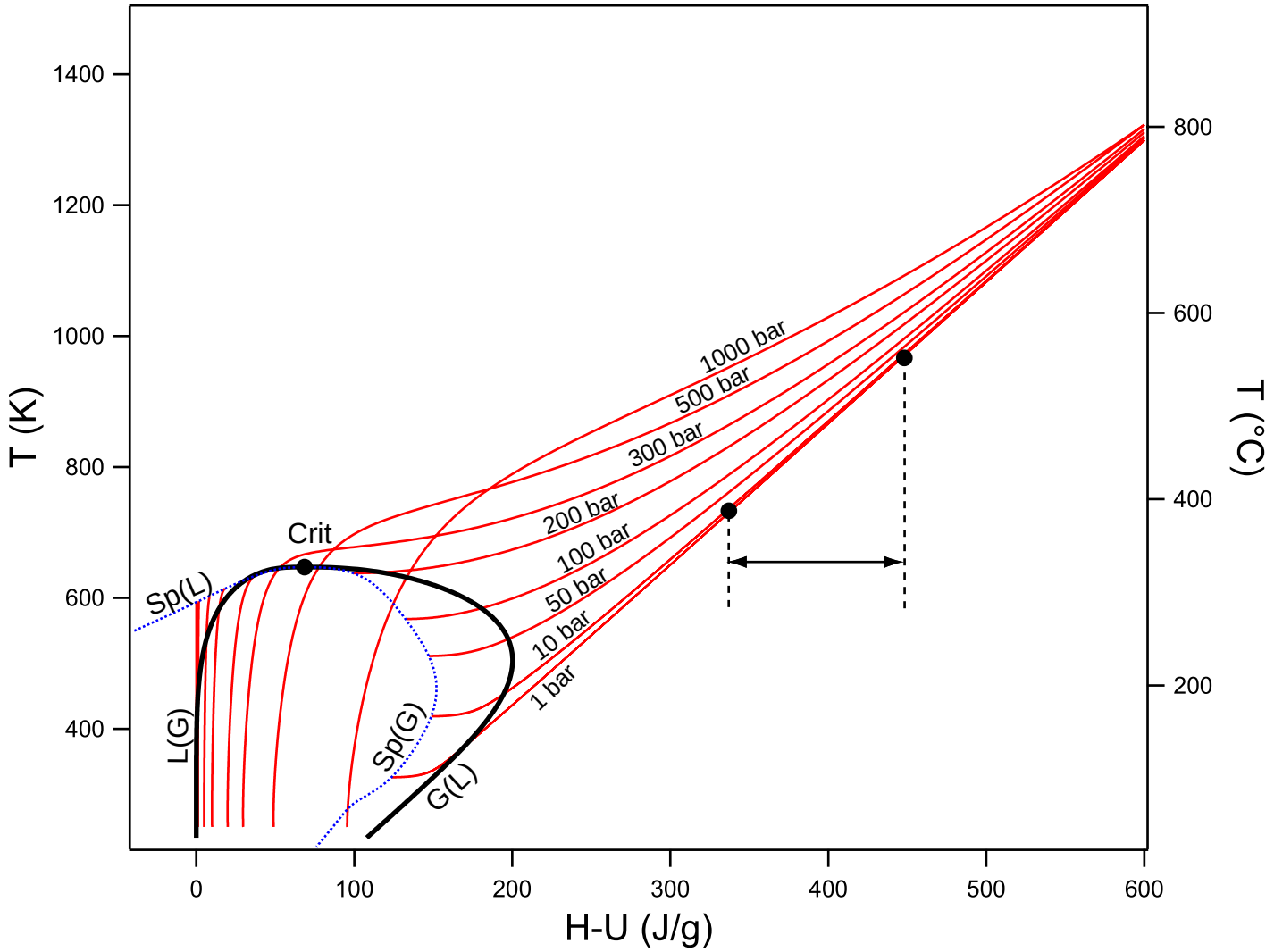
1400
1200
1000
800
600
400
T (K)
800
600
400
200
T (°C)
0
100
200
300
400
500
600
H-U (J/g)
1000 bar
500 bar
300 bar
200 bar
100 bar
50 bar
10 bar
1 bar
Crit
Sp(L)
L(G)
Sp(G)
G(L)

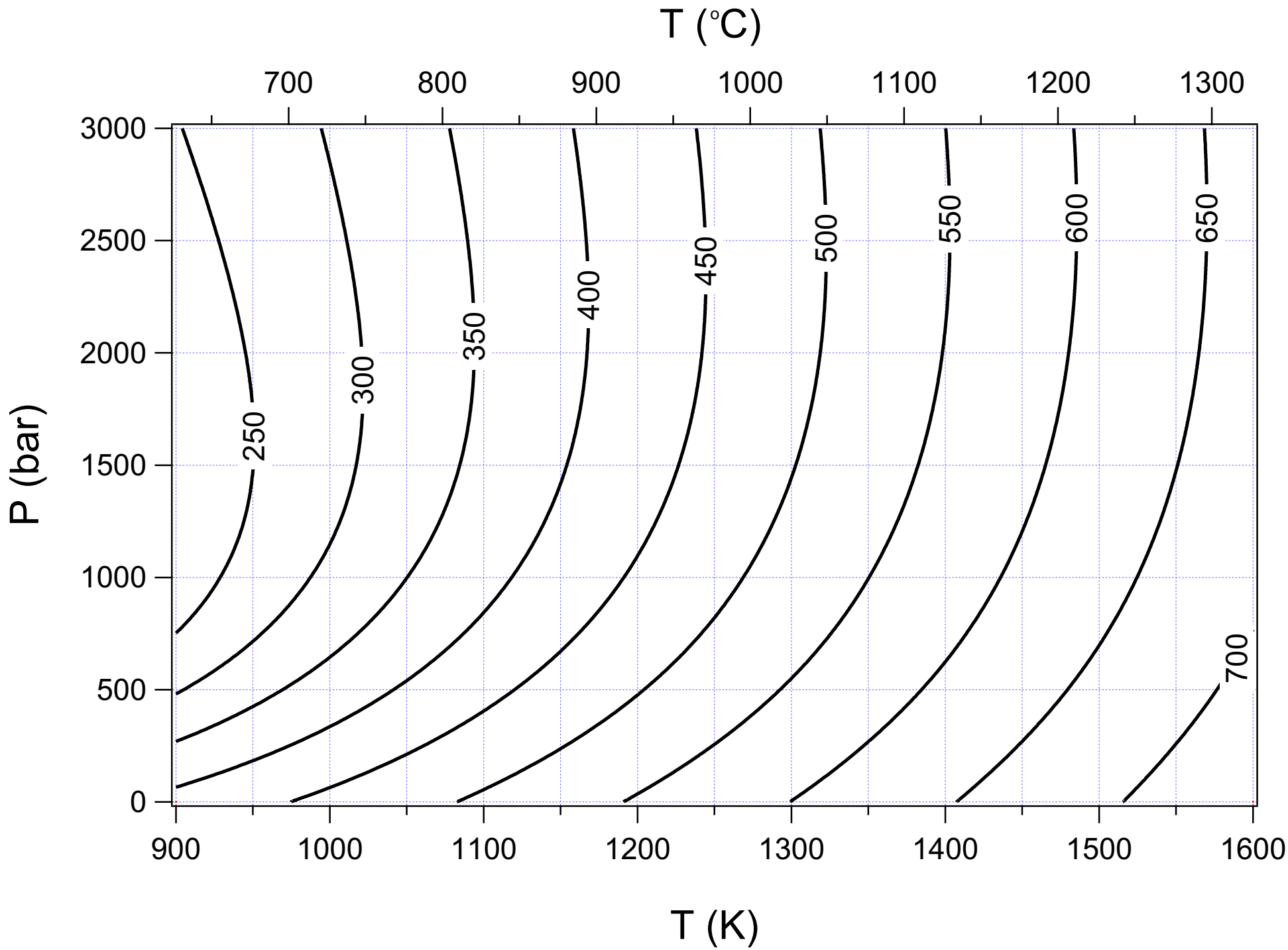
T (°C)
700
800
900
1000
1100
1200
1300
P (bar)
3000
2500
2000
1500
1000
500
0
250
300
350
400
450
500
550
600
650
700
900
1000
1100
1200
1300
1400
1500
1600
T (K)

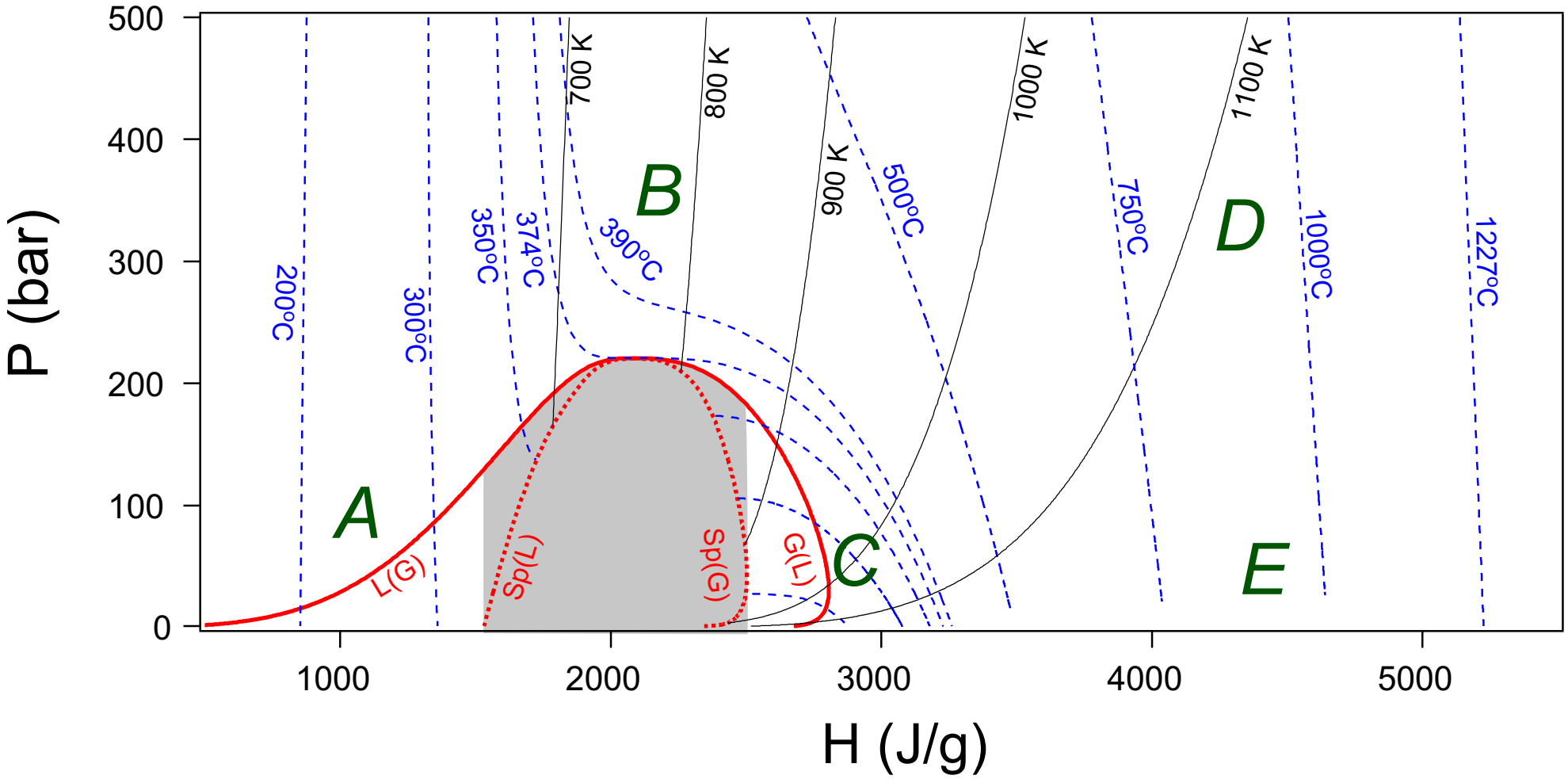
P (bar)
H (J/g)
500
400
300
200
100
0
1000
2000
3000
4000
5000
200°C
300°C
350°C
374°C
390°C
500°C
750°C
1000°C
1227°C
700 K
800 K
900 K
1000 K
1100 K
A
B
C
D
E
L(G)
Sp(L)
Sp(G)
G(L)